Modeling of a Milling and a Spiraling Circuit to Recover High Carbon-Ferro-Chrome from Slag

DISSERTATION

Prepared by

Refilwe Kopong (0400537k)

Submitted to

School of Chemical and Metallurgical Engineering, Faculty of Engineering and the Built Environment, University of the Witwatersrand, Johannesburg, South Africa

Supervisor(s): Prof S. Ndlovu and Prof V. Sibanda

June, 2015

Declaration

I declare that this dissertation is my own unaided work. It is being submitted for the Degree of Master of Science in Engineering in the University of the Witwatersrand, Johannesburg.

Abstract

High carbon ferrochrome (HCFeCr) alloy is the main source of chromium in steel making processes. During the production of high carbon ferrochrome alloy, in ferrochrome smelters, a substantial amount of slag is produced. These slags are generally disposed of in slag dumps or containment facilities causing environmental and containment problems. The slags have found limited use as aggregate for road surfacing and civil construction. With the renewed interest of exploiting secondary sources of metals, it has been found that most HCFeCr slags sitting in dumps contain a significant amount of alloy (Cr – 10% and Fe – 6 %) which can be recovered profitably if cheap reprocessing technology is applied.

In this study a circuit consisting of a mill and spiral concentrator was evaluated as a possible process route to recover the HCFeCr alloy trapped in the slag matrix. The focus of this present work was to model the mill and the spiral concentrator units using the experimental data generated in the earlier section of the research. Process modeling is crucial as a tool to simulate the plant process and optimize the conditions required for efficient operation. The material specific milling parameters namely the breakage function (B_{ij}) and the selection function (S_{ij}) were determined from the experimental data. The selection function was then used to estimate the parameters of the Austin model using the sum of squared errors. The Austin model parameters were found to be; a= 0.001, α= 4.9, Λ= 6.2 and μ= 3.1 and φi= 0.3, γ=0.6 and β= 5.7 respectively. These functions and parameters were incorporated into a batch milling population balance model to model particle size distribution of the mill product. The mill model predicted product size distribution from the mill at different milling conditions reasonably well. Milling conditions that gave an optimally liberated mill product were identified to be; powder filling of 60%, fraction of critical speed of 80%, ball size of 30mm and ball filling of 20%.

In modeling the spiral, two models were preferred, one by Lynch and Rao (1968) which considers that separation of particles in a spiral happens only because of the density difference of the particles and the other developed by Rao (2004) which takes into account both particle size and density. The two models reasonably predicted the experimental grade (17.21% Cr in concentrate) and recovery/yield of 41% obtained from a single stage rougher spiral test. The Rao (2004) model was however, superior in its prediction.

Acknowledgements

The author wishes to thank Prof. Vusumuzi Sibanda for his guidance, support and advice during this investigation. The author is also grateful to Prof. Sehliselo Ndlovu for her advice and support. The author would like to thank her mother, Mapula and siblings, Lebogang and Ofentse, for their continued support and encouragement.

Table of Contents

1. Introduction 1
2. Literature Review 6
   2.1. Recovery of values from waste 6
   2.2. Background on Ferrochrome 8
   2.3. Mineral Beneficiation 9
   2.4. Liberation 10
      2.4.1. Structure of the Grinding Mill 11
      2.4.2. Grinding Motion in a Mill 12
      2.4.3. Grinding Mechanisms 13
      2.4.4. Milling Kinetics 14
   2.5. Selection function 15
      2.5.1. Factors affecting the selection function 16
   2.6. Breakage function 21
   2.7. Population balance 22
   2.8. Gravity Concentration 23
      2.8.1. Spiral Concentrator 24
      2.8.2. Spiral Mechanism 26
      2.8.3. Modeling the spiral 28
3. Materials and Methods 31
   3.1. The High Carbon Ferro-Chrome Slag 31
   3.2. Batch Milling Test-work 31
      3.2.1. Categories of batch milling experiments performed on the mono-sized classes 32
   3.3. Single stage spiral testwork 33
4. Results and Discussion 36
   4.1. Assay by size 36
   4.2. Modeling Approach 37
      4.2.1 Estimating selection function using first order plots 37
      4.2.1.1 Effect of particle sizes on selection function 40
      4.2.1.2 Selection function at different conditions 43
   4.3. Breakage Function 46
   4.4. Particle size distribution 48
   4.5. Model optimization 50
   4.6. Spiral Modeling 51
      4.6.1. Model parameter estimation 52
      4.6.2. Modeling of the spiral using ball mill product distribution 59

5. Conclusions and recommendations 62
6. References 65
7. Appendices 69
7.1. Selection Function 69
7.2. Breakage Function 71
7.3. Particle size distribution 73
7.4. Model Optimisation 74
7.5. Spiral Modeling 75

List of Figures

Figure 1: Countries where chromite ore is produced (Murthy et al, 2011). 9
Figure 2: Grinding mill structure (Wills et al, 2006) 12
Figure 3: Motion in a mill (Wills et al, 2006) 13
Figure 4: Grinding mechanisms (a) impact and compression, (b) chipping and (c) abrasion (Wills et al, 2006). 13
Figure 5: Ore breakage 15
Figure 6: Spiral concentrator (Bayat et al, 2012) 24
Figure 7: Parameters of the spiral geometry (Doheim et al, 2013) 25
Figure 8: Forces acting on the particles in a spiral (Kapur et al, 1998) 27
Figure 9: Schematic diagram of a single stage spiral operation 28
Figure 10: Particle size distribution of the feed to the spiral 34
Figure 11: Chrome and iron content in the feed 37
Figure 12: First order plots for reference conditions 38
Figure 13: First order plots for 75% critical speed 38
Figure 14: First order plots 60% powder filling 39
Figure 15: Comparison between experimental and calculated selection functions for reference condition 42
Figure 16: Comparison between experimental and calculated selection functions for 75% critical speed 42
Figure 17: Comparison between experimental and calculated selection functions for 60% powder filling 43
Figure 18: Comparison between experimental and calculated selection function for all milling conditions 45
Figure 19: Cumulative breakage function for reference conditions 46
Figure 20: Cumulative breakage function for 75% critical speed 47
Figure 21: Cumulative breakage function for 60% powder filling 47
Figure 22: Experimental and predicted cumulative passing at Reference Conditions at 85% Critical Speed and 80% Powder Filling 48
Figure 23: Experimental and predicted cumulative passing at 75% critical speed 49
Figure 24: Experimental and predicted cumulative passing at 60% powder filling 49
Figure 25: Comparing optimal conditions to reference conditions 51
Figure 26: Partition Curve calculated using estimated model parameters 55
Figure 27: Partition Curve calculated using estimated model parameters 56

List of Tables

Table 1: Chromite, Ferro chrome, Stainless Steel end-use consumption and production (Watson, 2013)....2
Table 2: Different types of crushers (Coulson et al, 2002)....10
Table 3: Feed size and Product size for different crushers (Coulson et al, 2002) 11
Table 4: Head grade of the as received slag sample 31
Table 5: A range and reference values of main milling parameters used in the experiments .32
Table 6: Particle size distribution of the feed to the spiral 34
Table 7: Assays for each size class....36
Table 8: Experimental selection function from first order plots....39
Table 9: Parameters from Austin model....40
Table 10: Selection function calculated from the Austin model....41
Table 11: Parameters of the modified Austin Model....44
Table 12: Selection Function calculated from Modified Austin Model 44
Table 13: Average selection function model parameters....46
Table 14: Average breakage function model parameters 48
Table 15: Optimal operating conditions 50
Table 16: Results of the overall mass balance for the one stage spiral experiment....51
Table 17: Model parameters for first model (density only) – Lynch & Rao. (1968) 53
Table 18: Model parameters for second model (density and particle sizes) – Rao. (2004).....54
Table 19: Data for recovery and calculation using Lynch & Rao model (1968)....57
Table 20: Data for recovery and concentrate grade calculation using Rao model (2004).....58
Table 21: Comparison of the experimental and model recoveries 58
Table 22: Comparison of the experimental and model recoveries using optimized ball mill product 59

Nomenclature

Δ– multipliers model parameter =0.2

a - selection function model parameter constant

b_{ij} – the breakage function

B_{ij} is breakage distribution function and it's accumulative

C_1 – multiplier dependant on both ball and mill diameters

C_2 – multiplier dependant on only ball diameter

C_3 – multiplier dependant on only mill diameter

C_4 – multiplier dependant on ball and powder loading

C_5 – multiplier dependant on critical speed

d - ball diameter (mm)

D- mill diameter (m)

D_i – a mixing coefficient

f_c - mill filling (%)

J - fractional ball filling (%)

l – the space coordinate in the axial direction

m_k - weight fraction of balls of size k

η - model parameter constant

N_0 – multipliers model parameter ≈1

N_1 – multipliers model parameter ≈0.5

N_2 – multipliers model parameter ≈0.1 to 0.2

p_i is mass size fraction of size class i

S_A -selection function of component A (min^{-1})

S_B -selection function of component B (min^{-1})

S_i – the selection function (min^{-1})

$S_{i,k}$ - selection function for particle class i due to balls in the discrete size class k (min^{-1})

subscript T refers to the reference conditions

t is time (minutes)

U -powder filling (%)

u_i – the velocity of convective transport of particles in the axial direction (m/s)

w_i– the mass fraction of material in the i-th size class

x_i - maximum limit in the screen size interval i (mm)

α - selection function model parameter constant

β - breakage function model parameter that depend on the properties of the material

γ - breakage function model parameter

Λ - selection function model parameter constant

μ - selection function model parameter constant

ξ – model parameter constant

Φ - breakage function model parameter

φ_c -fraction of critical speed (%)

C- concentration (kg/hr)

CC - Concentration criterion

d - diameter of the particle (mm)

Df - specific gravity of the fluid medium (kg/m^3)

Dh - specific gravity of the heavy mineral (kg/m^3)

Dl - specific gravity of the light mineral (kg/m^3)

$e(d_p)$ - ideal classification function

F- feed (kg/hr)

F_n - normal components of all forces acting on a particle

g - gravitation constant (m/s^2)

h- Height loss (m)

H- Spiral height (m)

k_1 - experimentally determined constant

L(r)- Mainstream distance (m)

n- number of turns

P - dimensionless probability function

p - Parameter determining the sharpness of the partition surface

q - Parameter determining the sharpness of the partition surface

r- is the radial distance from the centerline axis (m)

R-angular distance in the mainstream direction from the spiral inlet (m)

r_i- inner radii (m)

r_o- outer trough radii (m)

u- Pitch) (m)

v - velocity of the particle (m/s)

W- Trough width (m)

x- ratio of $d_{particle}/d_{50}$ (ρ /ρ50)

Y -fraction of feed reporting to sink,

Y_p - pivot model parameter

α and m - sharpness of separation.

$\alpha(r)$ - Descent angle °

θ - local slope angle in the transverse direction °

λ - sharpness of classifications

ρ - density of the fluid (kg/m^3)

ρ_{50} - cut-off density (kg/m^3)

ρ_p, - pivot model parameter (kg/m^3)

σ - density of the particles (kg/m^3)

ψ – Curvature (dimensionless)

1. Introduction

High-carbon ferrochrome (HCFeCr) is an alloy of iron, chromium and carbon in which the carbon content is normally greater than 4% but less than 9%. High carbon ferrochrome (HCFeCr) is produced from chromite ore, mainly in submerged electric arc furnaces. The high chromite ore smelting process takes place at high temperatures and it essentially involves the reduction of chromium and iron oxides in the chromite ore using carbon and silica as reducing agents. Coal and/or coke are the common sources of carbon. The products from the smelting process are ferrochrome alloys and slag. HCFeCr alloy is mainly used as an alloying material in stainless steel making. Stainless steel production consumes 80% of the world's ferrochrome, mainly high carbon or charge grade ferrochrome (Murthy et al, 2011). The chromium in the HCFeCr is responsible for the improved hardness, toughness, resistance to oxidation, wear and corrosion in steels.

During the smelting process, a huge amount of electricity is consumed making production in countries with high power tariffs very costly. The world's ferrochrome production increased from 8.4 million tons in 2007 to 9.3 million tons in 2012 (Watson, 2013) as shown in Table 1. Most of the ferrochrome is produced in South Africa, China, India, Kazakhstan, Brazil, Finland, Oman, Russia and Turkey (Murthy et al, 2011).

With more ferrochrome being produced to meet the increasing demand of stainless steel, more ferrochrome slags will correspondingly be produced (Holappa et al, 2004). It is reported that for a ton of ferrochrome produced, 1.1-1.6 ton of slag is produced (Niemela et al, 2007). Ferrochrome slags have traditionally been used in road and civil engineering construction, and because of their superior chemical stability they have also found use in the production of refractories.

The main compounds in the HCFeCr slag are; SiO_2, MgO, Al_2O_3, Fe and Cr. A typical high carbon ferrochrome slag composition is 30 % SiO_2, 26 % Al_2O_3, 23 % MgO and 2 % CaO and about 5 - 10 % and 2 – 6 % of chromium and iron respectively (Niemelä, 2007). The chromium and iron content of the HCFeCr alloy, in most ferrochrome slags are high enough that the alloy can be recovered profitably especially when cheap gravity based concentrators are used.

Table 1: Chromite, Ferro chrome, Stainless Steel end-use consumption and production (Watson, 2013)

Chromite production and consumption (Mt)						
Production	**2007**	**2008**	**2009**	**2010**	**2011**	**2012E**
South Africa	9.7	9.7	6.9	10.9	10.2	11.0
Kazakhstan	3.7	3.6	3.3	3.8	3.8	3.8
India	3.3	3.9	3.8	3.8	3.9	3.8
Other Countries	4.8	6.6	5.3	5.2	5.5	5.3
Total Production	21.5	23.8	19.3	23.7	23.3	23.9
Apparent Global Consumption	20.9	18.7	14.6	22.2	23.0	23.3
Ferrochrome production and consumption (Mt)						
Production	**2007**	**2008**	**2009**	**2010**	**2011**	**2012E**
South Africa	3.6	3.2	2.2	3.6	3.3	3.0
China	1.4	1.3	1.3	2.2	2.8	3.3
Kazakhstan	1.2	1.0	1.0	1.2	1.1	1.1
India	0.8	0.8	0.7	1.0	1.0	0.9
Other Countries	1.5	1.4	1.2	0.7	1.0	1.0
Total Production	8.4	7.5	5.8	8.9	9.2	9.3
Total Global Consumption	7.6	6.8	6.7	9.0	9.6	9.7
Stainless Steel end-use consumption (Mt)						
Country	**2010**	**2011**	**2012**	**2013F**	**2014F**	**2015F**
EMEA	6.5	7.0	6.8	6.7	6.9	7.2
Americas	2.7	3.2	3.4	3.4	3.5	3.7
APAC	18.5	20.0	20.7	22.0	23.2	24.6
Global	27.7	30.2	30.9	32.1	33.6	35.5

The reasons for recovery of values from slag include; Shortage of chromite ores, environmental concerns of tailings and slags, increased demand for stainless steel requiring more chrome. In addition a metal-from-slag plant allows producers to cope with fluctuating ferroalloy markets. During times of low prices, a producer can shut down furnaces and rely on the low-cost metal-from-slag product to remain viable. When demand is high, the plant is a low-cost means to boost production thus allowing the company to sustain its activities. (Sripriya et al, 2005).

Gravity concentrators are preferred as the beneficiation techniques in that they are environmentally friendly (Wills et al, 2006). The effectiveness and efficiency of gravity concentrators is affected by many factors including the degree of liberation of valuable

minerals, specific gravity of various minerals and particle size distribution of the feed. For example, spiral concentrator separates at its greatest efficiency when its feed has particles in the size range of 75 microns to 1 mm and when there is narrow particle size distribution in the feed (Murthy et al, 2011). Slag dumps should therefore be milled to the desired particle size specifications prior to gravity concentration. Milling should achieve good liberation and generate an appropriate size distribution of the particles amenable to gravity concentration. High degree of liberation means the metal values are not locked inside other minerals.

Crushing and milling are done in order to liberate the metal in the slag as well as to reduce the particles to sizes suitable for concentration. In this research, a ball mill was used for wet batch milling of high-carbon ferrochrome slag dump samples to sizes of between 1 mm and about 75 microns. This size range has been shown to optimally liberate the values. The ball mill was selected as a best form of size reduction as it reduces sizes to less than 1 mm as required. The kinetics of milling was studied as it directly affects the final product from the mill. Milling kinetics describes the rate at which particles break and enable prediction of the product size distribution under certain operating conditions (Sonmez et al, 2010). The outputs from the milling kinetics study were used to develop a milling model that can describe the milling behavior of high carbon ferrochrome slag. Optimally liberated slag particles would then be fed into a spiral concentrator for recovery of values.

Spiral concentrator was proposed in this study as a concentration method to process the mill product to a saleable grade of ferrochrome concentrate because it can handle finely milled material more efficiently than other gravity concentration methods.

1.2 Problem Identification

In the production of high carbon ferrochrome alloy in smelters, a high amount of slag is produced. The disposed slags have been found to still contain an appreciable amount of high carbon ferrochrome alloy (HCFeCr) entrapped in the slag matrix which makes the slags a potential source of high carbon ferrochrome alloy through secondary processing of the slag dumps. The secondary processing of waste material like slags dumps has several benefits such as : environmental benefits through minimizing waste that reports to landfills, extension of the life of finite and in-elastic mineral resources by reducing primary mining of ores , use of cheaper and more environmental friendly methods to recover values.

The beneficiation practices of materials like ferrochrome slags have two major sections, which are comminution and concentration (Murthy et al, 2011). The comminution step deals with the crushing of the slag to liberate the high carbon ferrochrome alloy locked up in the slag matrix and further milling the material to make it amenable to the gravity concentration method chosen. The concentration step then upgrades the milled material in conventional gravity equipment like a spiral concentrator or a shaking table to a concentrate with greater than 45% Cr content in the HCFeCr alloy. This is a saleable grade of HCFeCr (Murthy et al, 2011).

High carbon ferrochrome slags are a re-constituted ore in a way, with their own characteristic mineralogy and slags are largely different depending on the smelting process and conditions applied during production. HCFeCr slags by nature of their production, which is conventionally by quenching of molten slag in water, are hard crystalline material with high abrasion indices. As a result, for beneficiation to occur successfully, the mineralogical composition of a particular slag dump needs to be understood. Further to that its crushing and milling characteristics have to be experimentally determined as they vary from one slag to another. In the preceding studies of this research, a slag sample from a high carbon ferrochrome smelter dump was crushed and milled and concentrated through spiraling. The data obtained from the milling and spiral concentration was utilized in this present study to model the milling and spiral concentration stages of the HCFeCr alloy recovery process.

1.3 Research objectives

- To calculate the main milling parameters, which are the Breakage and Selection functions for a specific high carbon ferrochrome slag sample from given milling data
- To use the milling parameters with a suitable milling model to predict the product size distribution of the mill at different operating conditions
- To compare the mill model predictions with available experimental data.
- To establish the optimum milling conditions that maximize the liberation of the high carbon ferrochrome slag
- To identify a suitable spiral concentration model and estimate the model parameters from experimental data
- To use the spiral model to predict the spiral concentrate grade and recovery and compare with measurements from a single stage rougher spiral concentration experiments

1.3.1 The research questions that will be answered after the modeling:

- What are the selection and breakage function parameters for this ferrochrome slag?
- What are the effects of particle sizes, change in critical speed and powder filling on the breakage rates?
- What particle size distribution is obtained using the model?
- What operating conditions are best to produce the most liberated particle sizes which are between the 1 mm and 75 microns?
- What are the model parameters for the identified spiral model?
- What recovery and grade of the high carbon ferrochrome slag can be obtained from a single rougher spiral stage?

2. Literature Review

2.1. Recovery of values from waste

The reserves of high grade ores are diminishing and therefore there is a need for exploration of other sources of high valuables minerals. There is a range of waste from a variety of industrial processes that contain metals that could potentially be recovered and these include; slag dumps, low grade ore dumps, fines dumps, electronic scraps, medical waste, metal finishing industry waste, spent petroleum catalysts, battery wastes, fly ash etc. (Jadhav et al, 2002).

These waste dumps possess risks which can include water pollution, contamination of land due to some heavy and hazardous metals in the waste and use of productive land. These wastes can however, be processed to recover valuable minerals present (Jadhav et al, 2002). Recovery of minerals from waste has become important as waste is considered a secondary resource with the added advantage of also conserving natural resources (Raghupathy et al, 2013). The recovery of value minerals from waste can be done if the method of recovery is cost effective. To recover these valuable metals, mineral processing techniques have been applied. These techniques include, pyrometallurgical, hydrometallurgical and bio-hydrometallurgical methods (leaching or roasting), separation, crushing and milling and flotation (Shen et al, 2003; Jadhav et al, 2002).

Recovery of metals using pyrometallurgical methods consists of the thermal treatment of the wastes which causes physical and chemical transformations. Some of the pyrometallurgical methods includes, calcining, roasting, smelting and refining. One of the methods of recovery of metals using hydrometallurgical methods is the leaching process. Leaching is done using a lixiviant in an aqueous solution. The metals are concentrated and purified using precipitation, cementation, solvent extraction and ion exchange. Biohydrometallurgy, which uses microbiological organisms like acidithiobacillus ferrooxidans, has been applied to treat waste as it is a low cost and environmentally friendly process (Jadhav et al, 2002).

The slags produced in metallurgical industry are generally classified as; ferrous slag, non-ferrous slag and incineration slag. Ferrous slag mainly includes iron slag or blast furnace

(BF) slag, steel slag, alloy steel slag and ferroalloy slag. The majority of the ferrous slags are blast furnace slags (BF slag) and steel slags. (Shen et al, 2002). BF slags are produced from the blast furnace during iron production and they contain iron of less than 2% so the slag is not reprocessed. However the slag is used in a variety of ways including cement production, road construction, civil engineering work etc. (Shen et al, 2002).

Steel slag is generated in a basic oxygen furnace and electric arc furnace during the steel making process. The method of mineral recovery from steel slag is dependent on the mineralogy of the slag among other things. The recovery methods applied include crushing or grinding, screening and magnetic separation. Alloy steel slags are similar to the BF slags and steel slags but they contain higher amounts of the minerals at low percentages. Nickel and chrome are the metals that are mostly recovered from this slag. These metals are recovered using magnetic or gravity separation. Some of the ferroalloy slags are FeMn slag, SiMn slag and CrFe (charge chrome) slag etc. The methods that are used to recover values from the latter slags include magnetic separation or gravity separation. However, no commercial operation using magnetic separation has been documented. Jigging has been used to recover coarse materials of size (-5 mm, -10mm) and shaking tables have been used for the finer particles. Some commercial plants have been built to recover ferrochrome from slag in South Africa, in such plants jigging has been used for the coarse material (- 25+1 mm) and spiral for the fine fraction (-1 mm) (Shen et al, 2002). The process recovered about 55% chromium from an 11% chromium in the feed (Shen et al, 2002).

There are many different types of non-ferrous slags which are generated from non-ferrous smelters. These include copper slags which are generally processed using flotation, leaching and roasting. The salt slags are produced from the aluminum industry. The value recovery process for the salt slags has five major steps, which are; metal separation, leaching, solid liquid separation, gas treatment and, evaporation and crystallization (Shen et al, 2002). Incineration slag mostly includes municipal slag from incineration processes. Values from incineration slag can be recovered by mechanical separation, or special treatments, such as re-melting and extraction using acid or other solvents (Shen et al, 2002).

2.2. Background on Ferrochrome

Chromite ore is an important raw material in the production of ferrochrome alloys. It occurs as chromium spinel which contains magnesium, iron and aluminum in varying compositions depending on the deposit. Gangue associated with the chromite ore includes talc, hematite, goethite and quartz. During the ferrochrome alloy production, slag is also produced. Slag contains considerable amount of ferrochrome that can be recovered (Niemelä, 2007).

The supply of chrome ores used in the production of ferroalloys for making stainless steel is under considerable strain owing to the high demand of stainless steel. Stainless steel production uses 80% of the ferrochrome that is produced, mainly high carbon or charge grade ferrochrome (Murthy et al, 2011). The typical high carbon ferrochrome slag composition is 30 % SiO_2, 26 % Al_2O_3, 23 % MgO and 2 % CaO and about 5 – 10 % and 2 – 6 % of chrome and iron respectively (Niemelä, 2007).

Most of the world's chromite ore is produced in South Africa (39%), India (16%), Kazakhstan (15%), Brazil, Finland, Oman, Russia and Turkey accounting for 21% (Murthy et al, 2011). See Figure 1. The world's ferrochrome production has increased from 8.4 million tons in 2007 to 9.3 million tons in 2012 (Watson, 2013). Stainless steel production is also expected to increase (Watson, 2013) especially driven by the booming Chinese economy.

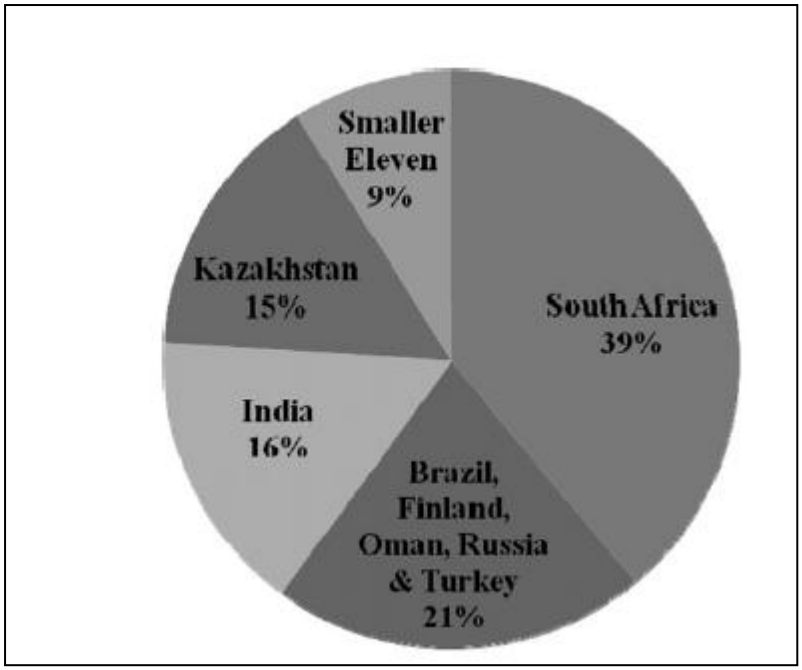

Figure 1: Countries where chromite ore is produced (Murthy et al, 2011).

The critical issues that affect the production of chrome include treating low grade chromite ore, recovery of ultrafine chrome, reduction of tailings, reprocessing of tailings and slags, and the concentration of the chromite content (Murthy et al, 2011). There are three types of waste that are produced during the production of ferrochrome alloys. These are the slags which are produced during the smelting process, the bag filter dust which is generated during the cleaning of the off-gas and the sludge produced during the scrubbing of the off-gas from the furnaces (van Staden et al, 2014).

Ferrochrome slag can be processed using crushers and wet magnetic and gravimetric methods (Erdem et al, 2005), crushing using primary and secondary crushers, jigging and tabling (Sripriya et al, 2005), spiral concentrator and shaking tables (Murthy et al, 2011).

2.3. Mineral Beneficiation

Mineral beneficiation or processing is a major component in the value chain for the production of final metal products. Mineral beneficiation consists of the manipulation of the physical properties of the ore to produce desired particles size leading to the liberation of the mineral from the gangue material. It is also used to control the particle size in the preparation of feed to consecutive processing stages. It consists of size reduction (or comminution) which

is liberation of minerals by crushing and grinding (Wills et al, 2006). This is normally followed by the concentration step which is the separation of minerals by various units of operation.

Some of the techniques used to separate minerals include sorting i.e. making use of optical or other properties of the mineral or gangue which could be done by hand or machines. Separation using density properties is also common; the methods include gravity concentrators and dense medium separators. Separation can also be achieved using surface properties of the minerals e.g. froth flotation. Magnetic properties of the minerals and electrical conductivity properties can also be exploited to effect separation (Wills et al, 2006).

In mineral processing the ore is normally handled in slurry form making dewatering one of the essential steps for the removal of water using specific unit operation like thickening and filtration to prepare the ore material for downstream processing. Once the ore is concentrated, it can be processed further using chemical methods, which can include hydrometallurgy or pyrometallurgy.

2.4. Liberation

Size reduction is important in the liberation of valuable mineral for further processing. Unit operations for liberation include coarse, intermediate and fine crushers as listed in Table 2.

Table 2: Different types of crushers (Coulson et al, 2002)

Coarse Crushers	**Intermediate crushers**	**Fine crushers**
Stag jaw crusher	Crushing rolls	Buhrstone mill
Dodge jaw crusher	Disc crusher	Roller mill
Gyratory crusher	Edge runner mill	NEI pendulum mill
Other coarse crusher	Hammer mill	Griffin mill
	Sing roll crusher	Ring roller mill (Loculco)
	Pin mill	Ball mill
	Symons disc crusher	Tube mill
	Standard cone crusher	Hardinge mill
		Babcok mill

Table 3 shows that different crushers work better at different feed size of particles. The coarse crushers are used for bigger particles while the fine crushers are used for smaller particles sizes.

Table 3: Feed size and Product size for different crushers (Coulson et al, 2002)

Crushers	**Feed sizes**	**Product sizes**
Coarse Crushers	1500-40 mm	50-5 mm
Intermediate crushers	50-5 mm	5-0.1 mm
Fine crushers	5-2 mm	0.1mm

Crushing

In comminution, crushing is normally the first mechanical stage. Its primary objective is to liberate the valuable mineral from the gangue. Crushing can occur in several stages and the feed particle sizes can be as large as 1.5m. Primary crushing is normally done underground to reduce the particle size of the run of mine to a size that is suitable for transportation. The products of the primary crusher are further crushed in a secondary crusher and tertiary crusher if required. (Wills et al, 2006).

Milling

Milling also known as grinding is the last stage of comminution. (Wills et al, 2006). Milling is usually applied when downstream processes require very small particles that are in the micron range. The average particle size range for the feed as well as the product is as shown in Table 3

2.4.1. Structure of the Grinding Mill

The structure of the mill consists of a shell, which is made from rolled steel plates and designed to sustain impact and heavy loading. The main components of the mill are mill ends, trunnions and bearings, liners, mill feeders, drum feeders, and combination drum-scoop feeders (Wills et al, 2006) as seen in Figure 2 below.

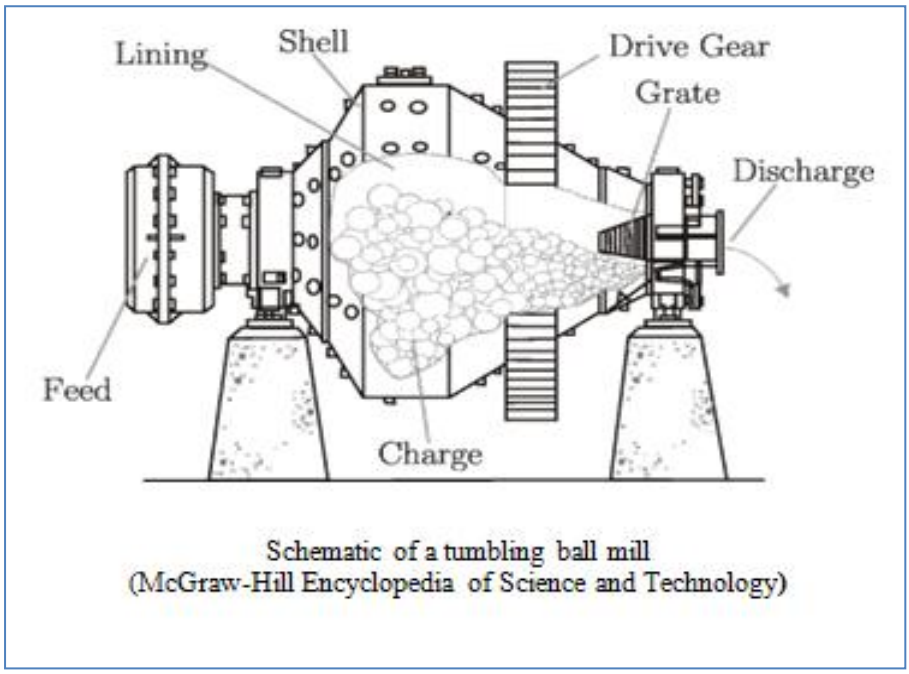

Figure 2: Grinding mill structure (Wills et al, 2006)

2.4.2. Grinding Motion in a Mill

Figure 3 (Wills et al, 2006) shows the motion of the mill whereby the grinding media (balls in the case of the ball mill) is lifted along the rising side of the mill, due to the friction of the mill shell and the rotation of the mill. This happens until a position of dynamic equilibrium is reached. The media then cataracts down the free surface of other media in the mill, down to the toe of the mill (Wills et al, 2006). The speed at which the mill is run is very critical as it affects the product size distribution as well as the wear on the liners inside the mill. At low speeds, abrasive comminution occurs in which the media tends to roll down the toe of the mill. This is called cascading and it produces a lot of fines and results in wear of the liners. At high speeds, impact comminution occurs. This is called cataracting and it produces coarse particles. (Wills et al, 2006).

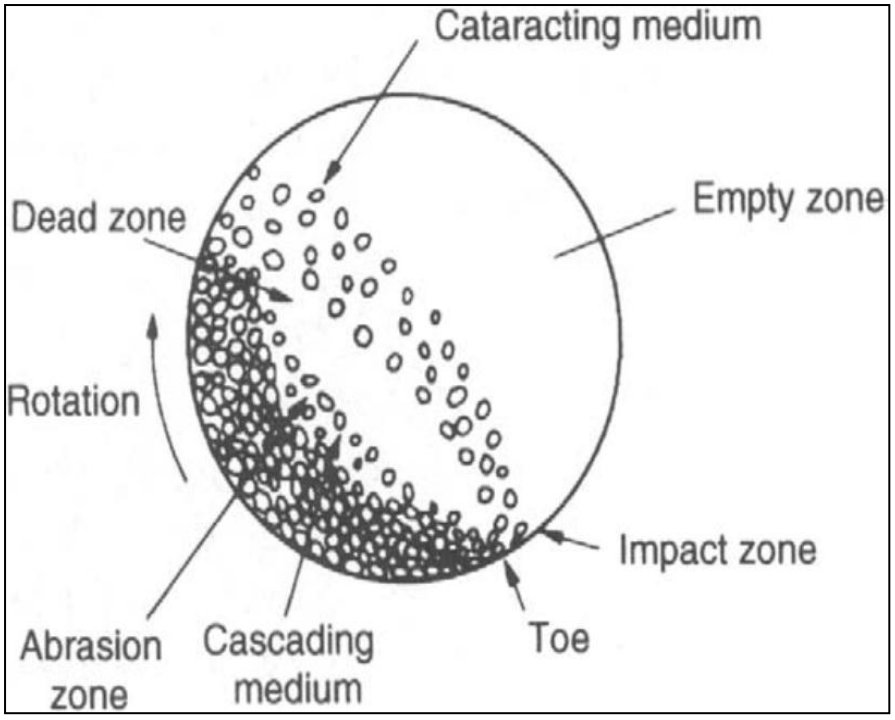

Figure 3: Motion in a mill (Wills et al, 2006)

2.4.3. Grinding Mechanisms

There are several grinding mechanisms involved during the milling process. These includes impact or compression whereby forces are applied to the particle normally as seen in Figure 4 (a), chipping which is due to oblique forces as seen in Figure 4 (b) and abrasion which are forces acting on the particles parallel to its surface as seen in Figure 4 (c), (Wills et al, 2006). Grinding media includes steel rods, steel balls, and large rocks from the ores itself.

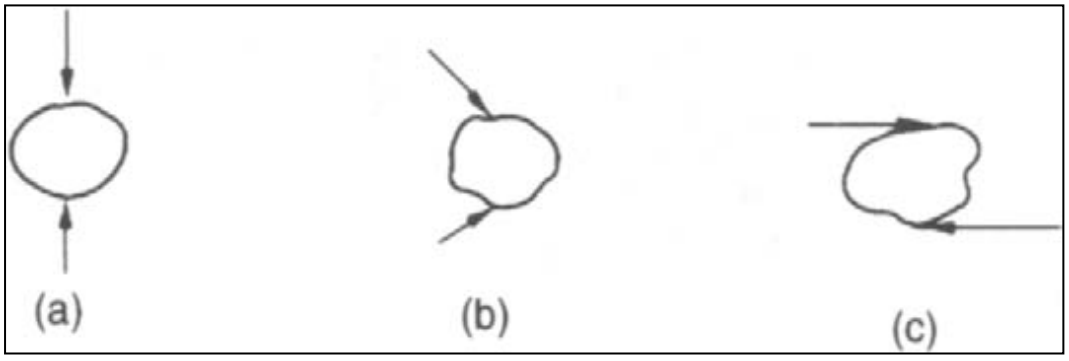

Figure 4: Grinding mechanisms (a) impact and compression, (b) chipping and (c) abrasion (Wills et al, 2006).

2.4.4. Milling Kinetics

Ores from the mines, materials like slags and dumps, to be milled normally consists of different sizes; from coarse material to fines. Specific cut off sizes are normally required for the downstream processes like leaching, flotation etc. It is important to classify ores into different sizes and standard screens are normally used for classification of coarse materials and hydrocyclones for finer materials.

A ball mill model is simulated to predict product size distribution as a function of mill design and operating conditions (Sonmez et al, 2010). To construct such a model, the rate at which the particles break into smaller size particles as well as the fraction that is broken needs to be known. The selection function and breakage function are used in this particular case. These functions are explained below.

- The selection function represents the selection of a fraction of the material to be broken, where selection function (also known as the probability of breakage or specific breakage rate) is denoted as S_i, where i=1,2,…,n
- The breakage function represents the breakage of the selected material producing a given distribution of fragment sizes, where breakage function (also known as distribution function) is denoted by b_{ij} where $n \geq i \geq j \geq 1$, where n is the number of the size classes (Monov et al, 2012)

The functions stated above can be represented in Figure 5 (Monov et al, 2012). The feed size is shown on the left column. During the grinding process the feed progressively breaks into smaller sizes as shown by arrows, and the products are shown in the last column. The total mass of the material stays the same throughout the process (Monov et al, 2012).

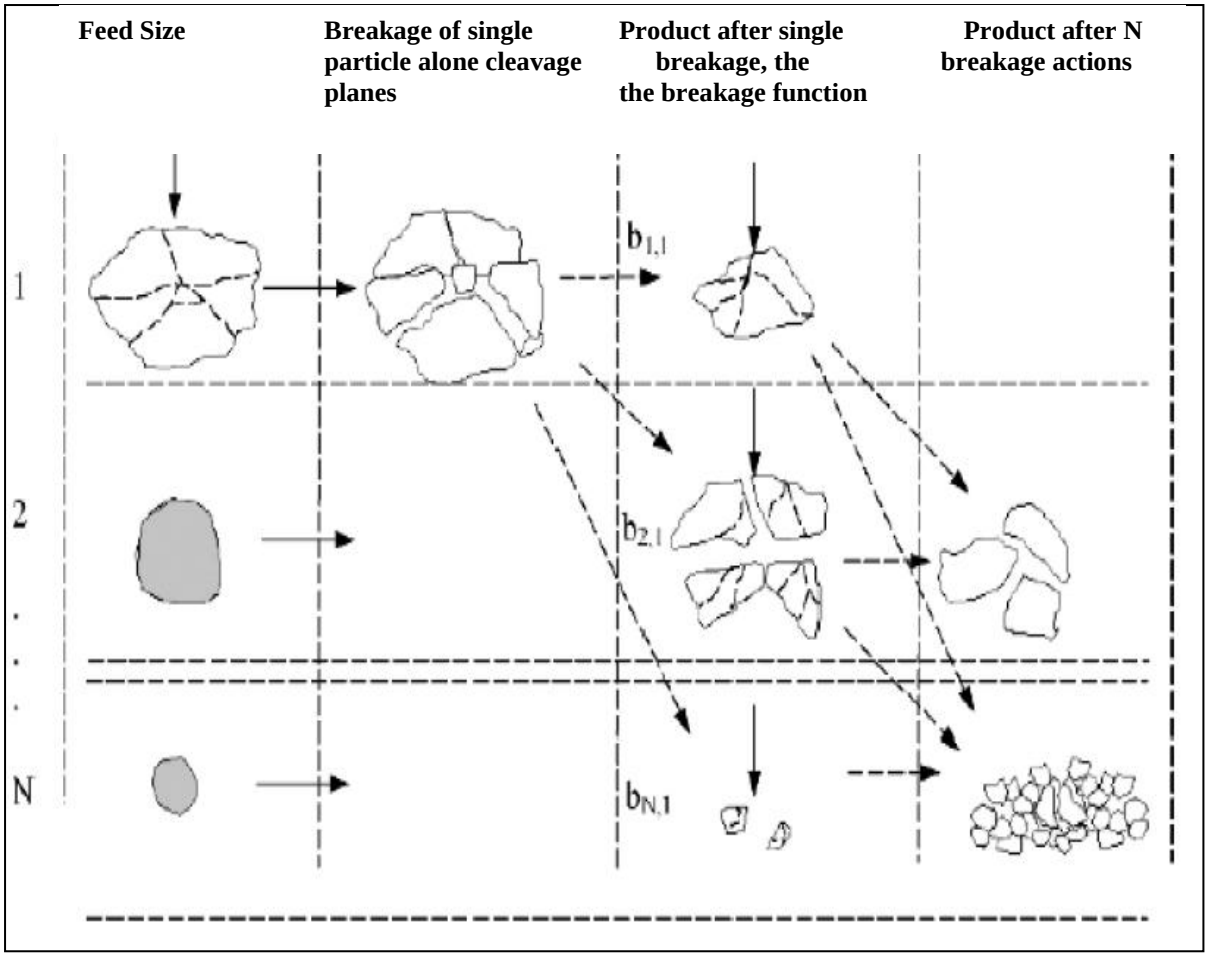

Figure 5: Ore breakage

Selection and breakage functions depend on the mill design, operating conditions as well as the properties of the material. These are explained in section 2.5 and 2.6 below.

2.5. Selection function

When an ore is milled, it breaks into smaller classes. Each class breaks into the next class and this follows, in principle, first order law. The selection function (S) indicates the rate of breakage of each specific size class. The following equation is used to calculate the selection function (Sonmez et al, 2010, Austin et al, 1984).

$$\frac{d(wp_i)}{dt} = -S_i wp_i \qquad \text{Equation 2.1}$$

From t (0) to t integrates to

$$\log p_i(t) = \log p_i(0) - \frac{S_i t}{2.3}$$ Equation 2.2

Where p_i is mass size fraction of size class i

t is time

A plot of log p_i (t) against time will result in a straight line. The slope of which is $-S_i/2.3$. Alternatively a plot of log p_i (t)/p_i (0) against time will give a slope of $-S_i$.

If breakage departs from the first order kinetics, abnormal breakage occurs (Chimwani et al, 2013). Some materials consist of an initial material component A which in turn breaks into another material B (Chimwani et al, 2013)). The following equation shows the non-first order batch grinding model which was proposed by Austin (1977)

$$w_i(t) = \frac{m(t)}{m(0)} = (1-\phi_i)e^{-S_A t} + \phi_i . e^{-S_B t}$$ Equation 2.3

where

$$\phi = \frac{b'_{ii}\, S_A}{S_A - S_B}$$

Where S_A and S_B are selection functions of component A and B of the material respectively.

2.5.1. Factors affecting the selection function

The selection function and the overall mill performance are affected by particle size, powder filling (U), fractional ball filling (J), fraction of critical speed (φ_c) and ball diameter (d). These factors are explained below

2.5.1.1. Effect of particle sizes on selection function

The selection function can also be calculated using the empirical formula (Sonmez et al, 2010, Austin et al, 1984). Equation 2.4 is used to estimate selection function at different particle sizes;

$$S_i = a.x_i^{\alpha}.\frac{1}{1+\left(\frac{x_i}{\mu}\right)^{\Lambda}}$$ Equation 2.4

where x_i is the maximum limit in the screen size interval i in mm, Λ and α are characteristic constants which are dependent on ore properties, a is dependent on the mill conditions and can also depend on the material properties and μ is characteristic constant dependent on mill conditions (Chimwani et al, 2013 , 2014).

Equation 2.4 is only applicable for different particle sizes but at the same milling conditions. If milling conditions change then the selection function equation should show this. This will be looked at in the subsequent sections (sections 2.5.1.2 to 2.5.1.5). Equation 2.4 can also be written in the form shown in equation 2.5 to include the changes in milling conditions. This equation can be used for scaling up from laboratory to industrial milling conditions (Sonmez et al, 2010, Chimwani et al, 2014). These conditions will be described in the next sections (sections 2.5.1.2 to 2.5.1.5).

$$S = ax_i^{\alpha}[\frac{1}{1+(\frac{x_i}{C_1\mu})^{\Lambda}}]C_2C_3C_4C_5$$ Equation 2.5

Where C_1 to C_5 are multipliers that show how selection function changes with milling conditions. C_1 is dependent on both ball and mill diameters, C_2 on only the ball diameter, C_3 on only the mill diameter, C_4 on ball and powder loading and C_5 on the critical speed (Sonmez et al, 2010). Chimwani et al, (2014), expanded a and μ similarly in equation 2.5, as seen in the following section 2.5.1.2.

2.5.1.2. Effect of ball size and ball mill diameter

The parameters above a and μ (equation 2.5) which were described as being dependant on mill conditions, both depend on ball sizes and ball mill diameter (d).

Austin et al, 1984 had the similar formula for the effect of ball sizes in the following form (Katubilwa et al, 2011)

$$a = \left(\frac{d_T}{d}\right)^{\xi} \qquad \mu = \left(\frac{d}{d_T}\right)^{\eta}$$ Equation 2.6

where ξ and η are parameter constants. Chimwani et al (2014), states that the value of η is between 1 and 2. The subscript T refers to the reference conditions.

The multipliers in equation 2.5 for the effect on ball and mill diameters are described below

The following relationships can be described (Sonmez et al, 2010)

$$C_1 = \left(\frac{D}{D_T}\right)^{N_2}\left(\frac{d}{d_T}\right)^{2}$$ Equation 2.7

$$C_2 = \left(\frac{d_T}{d}\right)^{N_0}$$ Equation 2.8

$$C_3 = \left(\frac{D}{D_T}\right)^{N_1} \quad \text{D<3.81}$$

$$C_3 = \left(\frac{3.81}{D_T}\right)^{N_1}\left(\frac{D}{3.81}\right)^{N_1-\Delta} \quad \text{D}\geq 3.81$$ Equation 2.9

Where constants $N_0 \approx 1$, $N_1 \approx 0.5$, $N_2 \approx 0.1$ to 0.2 and $\Delta = 0.2$ for larger mills. D is for mill diameter (Sonmez et al, 2010)

2.5.1.3. Effect of critical speed

Mill speed has an effect on the breakage rates. Critical speed is the theoretical speed at which the balls rotate. It is given by the following equation (Chimwani et al, 2014).

$$\phi_c, rpm = \frac{42.2}{\sqrt{D-d}}$$ Equation 2.10

C_5 from equation 2.5 can be described below

$$C_5 = \left(\frac{(\phi_c - 0.1)}{(\phi_{cT} - 0.1)}\right)\left(\frac{1+\exp[15.7(\phi_{cT} - 0.94)]}{1+\exp[15.7(\phi_c - 0.94)]}\right)$$ Equation 2.11

A critical speed of between 70% and 80% was found to give the best breakage rates (Chimwani et al, 2014).

Deniz, 2004 studied the effects of mill speed on the kinetic breakage parameter of clinker and limestone. The results from the study showed that, the higher the mill speed, the higher the selection function. The following equation 2.12 was used to calculate a_T for different samples.

$$a_T \ \alpha \ \frac{\phi_c - 0.1}{1 + \exp[15.7(\phi_c - 0.94)]} \qquad \text{Equation 2.12}$$

2.5.1.4. Effect of ball and powder loading

Ball filling (J) is the volume of the mill which is filled by the balls at rest. The following equation shows how ball filling can be calculated when assuming that the porosity of the bed is 0.4 (Chimwani et al, 2014).

$$J = \frac{\left(\frac{Mass\ of\ balls}{Ball\ density}\right)}{Mill\ Volume} x \frac{1}{(1 - 0.4)} \qquad \text{Equation 2.13}$$

Chimwani et al, (2014) state that the rate of breakage is dependent on the ball filling in the mill. The rate of breakage increases when ball filling is increased, but then decreases after a maximum is reached. In practice, the optimal level of operation is normally between 20% and 40%.

Powder loading (U) is explained as the fraction of spaces between the balls. This has a relationship between mill filling (f_c) and ball filling as seen in the following equation. Mill filling (f_c) is the volume of the mill which is filled by the powder at rest. U of between 0.6 and 1 will normally give an efficient rate of breakage (Chimwani et al, 2014).

$$U = \frac{f_c}{0.4J} \qquad \text{Equation 2.14}$$

Increasing powders in the mill fills the collision space between the balls and results in a higher breakage rate (Lameck, 2005). However, over-filling a mill will result in an effect called powder cushioning, which will decrease the rate of breakage (Chimwani et al, 2014).

C_4 from equation 2.5 can be described below (Sonmez et al, 2010)

$$C_4 = \left[\frac{1+6.6J^{2.3}}{1+6.6J_T{}^{2.3}}\right]\exp(-c(U-U_T)) \qquad \text{Equation 2.15}$$

where c is 1.2 and 1.32 for dry and wet grinding respectively (Lameck, 2005)

The combined relationship between the ball mill diameter, powder and ball loading on the parameter a in equation 2.4 (Chimwani et al, 2014) is shown below

$$a = a_T\left(\frac{D}{D_T}\right)^{0.5}\left(\frac{1+6.6J_T{}^{2.3}}{1+6.6J^{2.3}}\right)\exp\left[1-c(U-U_T)\right] \qquad D\leq 3.8\text{m} \qquad \text{Equation 2.16}$$

$$a = a_T\left(\frac{3.8}{D_T}\right)^{0.5}\left(\frac{D}{D_T}\right)^{0.3}\left(\frac{1+6.6J_T{}^{2.3}}{1+6.6J^{2.3}}\right)\exp\left[1-c(U-U_T)\right] \qquad D>3.8\text{m}$$

2.5.1.5. Effect of ball size distribution

Austin, 1984 estimated the effect of ball size distribution on the overall selection function. The mean value of S is given by

$$\overline{S}_i = \sum_{k=1}^{m} S_{i,k}\, m_k \qquad \text{Equation 2.17}$$

where m_k is the weight fraction of balls of size k and $S_{i,k}$ represents the selection function for particle class i due to balls in the discrete size class k (Katubilwa et al, 2011).

2.6. Breakage function

The breakage function indicates how particles break into other smaller sizes. It is calculated using the following formula (BII method) (Chimwani et al, 2013, Austin et al, 1984).

$$B_{ij} = \frac{\log\left[\left(1-p_i(0)\right)/\left(1-p_i(t)\right)\right]}{\log\left[\left(1-p_{j+1}(0)\right)/\left(1-p_{j+1}(t)\right)\right]} \qquad i>j \qquad \text{Equation 2.18}$$

Where B_{ij} is breakage distribution function and it's accumulative

Once B_{ij} is calculated, b_{ij} is then calculated by subtraction. $B_{ij} = \sum_{k=n}^{i} b_{k,j}$

This method is used for one size class. B_{ij} can be determined when the grinding duration is such that only 20-30% breakage occurs in the top size. This is to minimize re-breakage.

An empirical model used to calculate the breakage function is shown below (Sonmez et al, 2010) and (Austin et al, 1984).

$$B_{ij}(\ell_i, \ell_j) = \phi_j \left(\frac{\ell_i}{\ell_{j+1}}\right)^{\gamma} + (1-\phi_j)\left(\frac{\ell_i}{\ell_{j+1}}\right)^{\beta} \qquad \text{Equation 2.19}$$

Where γ is gamma

Φ is phi

β is beta

γ, Φ and β are the model parameters that depend on the properties of the material. The values for these parameters are generally greater than 0.6 for γ, between 0 and 1 for Φ and greater than 2.5 for β (Chimwani et al, 2013). The breakage distribution function can be considered normalisable, meaning that it's not a function of the initial particle size. This assumption has been proven for many materials and has been used for simulation purposes (Chimwani et al, 2013).

2.7. Population balance

There are different types of models that can be used for modeling of mills. These include, the matrix model, size-mass balance kinetic model, population balance kinetic model, multi-segment kinetic model and cumulative basis kinetic model (Anaç, 1994). This report will focus on the population balance model (PBM).

Population balance model is used to model the milling process. It uses the selection and breakage functions that have been described in the preceding section. There are several assumptions that are made in modeling of the milling process, these include: (i) that the mill is perfectly mixed in the radial direction but only partial in the axial direction, (Toneva et al, 2007), (ii) that the contents in the mill are uniform and that the particles of different sizes are broken in similar way (Monov et al, 2002) (iii) that no agglomeration processes take place during the grinding/milling (Monov et al, 2002).

The population balance kinetic model for the grinding process in the case of breakage is expressed as

$$\frac{dw_i(l,t)}{dt} = -S_i w_i(l,t) + \sum_{j=1}^{i-1} S_j b_{i,j} w_j(l,t) + D_i \frac{d^2 w_i(l,t)}{dl^2} - u_i \frac{dw_i(l,t)}{dl} \qquad \text{Equation 2.20}$$

where

t is the grinding time;

l – the space coordinate in the axial direction;

w_i– the mass fraction of material in the i-th size class;

b_{ij} – the breakage function;

S_i – the selection function;

D_i – a mixing coefficient;

u_i – the velocity of convective transport of particles in the axial direction.

Assuming that the batch mill is perfectly mixed the equation then becomes (King, 2000)

$$\frac{dw_i(t)}{dt} = -S_i w_i(t) + \sum_{j=1}^{i-1} S_j b_{i,j} w_j(t) \qquad \text{Equation 2.21}$$

For a continuous mill, equation becomes

$$Wp_i^P = Wp_i^F + M\sum_{j=1}^{i-1} b_{ij} S_j m_j - MS_i m_i \qquad \text{Equation 2.22}$$

$$p_i^P = p_i^F + \tau\sum_{j=1}^{i-1} b_{ij} S_j m_j - \tau S_i m_i \qquad \text{Equation 2.23}$$

Where τ=M/W, and for a perfectly mixed mill $m_i=p_i^p$

$$p_i^P = p_i^F + \sum_{j=1}^{i-1} b_{ij} \tau S_j p_j^p - \tau S_i p_i^p \qquad \text{Equation 2.24}$$

$$p_i^P = \frac{p_i^F + \sum_{j=1}^{i-1} b_{ij} \tau S_j p_j^p}{1 + S_i \tau} \text{ for all i} \qquad \text{Equation 2.25}$$

2.8. Gravity Concentration

Gravity concentration uses the different specific gravities of the minerals for separation. Gravity concentrators mostly use air or water as a fluid medium. For separation to occur there has to be differences in the densities between the gangue material and the value mineral. Concentration criterion (CC), is a formula that is used to have an idea if separation is possible and to what degree (Wills et al, 2006).

Concentration criterion $CC = \frac{(D_h - D_f)}{(D_l - D_f)}$ Equation 2.26

where D_h is the specific gravity of the heavy mineral, D_l is the specific gravity of the light mineral, and D_f is the specific gravity of the fluid medium.

If CC is greater than 2.5, whether negative or positive, then separation is relatively easy. The lower the CC value the more difficult the separation. The efficiency of separation is not only dependent on the density of the minerals but also on the particle sizes. The larger the particles sizes, the higher the gravity separation efficiency. From practice, the feed particles sizes to the gravity concentrator must be closely controlled so that size effect is eliminated and the separation is only dependent on the specific gravities (Wills et al, 2006).

If a feed material has same densities but different particles sizes, then classification is a more relevant type of separation. The separation would be based on cut-off particle size. If a feed material has similar particle sizes but different densities then concentration is more relevant type of separation and the separation would be based on cut-off density. If a feed material has different particle sizes and densities then a combination of classification and concentration is more relevant, where a screen can be used to narrow size ranges and then a concentration step can follow (Wood, 2007).

There are a number of different gravity concentrators that are used in industry. These include jigs, shaking tables, sluices, spirals and hydrocyclones.

2.8.1. Spiral Concentrator

A spiral concentrator was proposed in this study as a concentration method to process the slag mill product to a saleable grade of ferrochrome concentrate because it can handle finely milled material more efficiently than other gravity concentration methods. A spiral is an open channel, which consists of a trough that twists downwards in the form of a vertical circular helix about a central axis as shown in Figure 6 (Kapur et al, 1999 and Tripathy et al, 2012). .

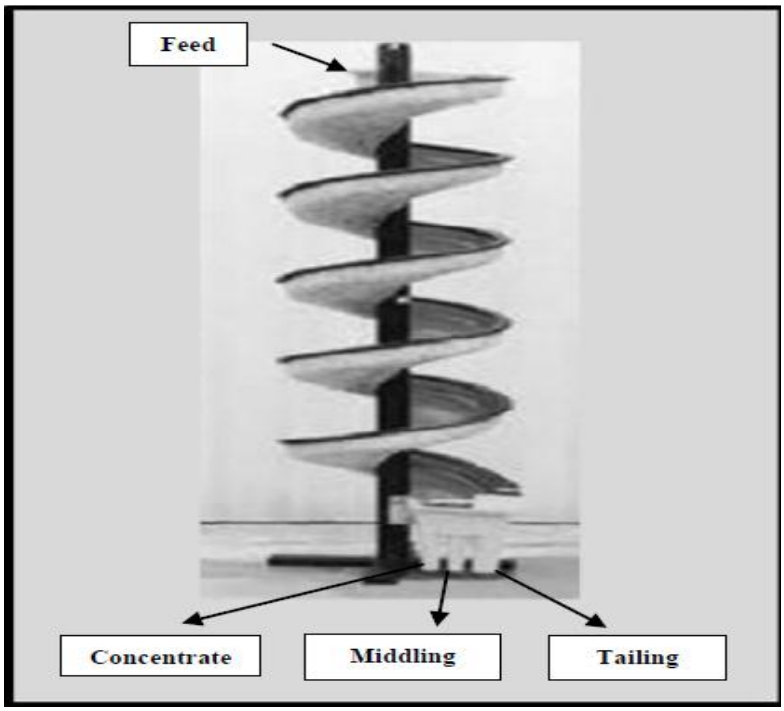

Figure 6: Spiral concentrator (Bayat et al, 2012)

The performance of a spiral depends strongly on its physical/structural and process design parameters. The structural design parameters include its diameter, height, number of turns, pitch and slope and shape of the channel or trough and its dimensions (Kapur et al, 1998). The equations for these structural design parameters are listed below (Doheim et al, 2013):

- Pitch: $u = 2\pi\, r \tan(\alpha)$ (m)
- Curvature: $\psi = (r_i + r_o)/2W$ (dimensionless)
- Descent angle: $\alpha(r) = \tan^{-1}(u/2\pi\, r)$ °
- Trough width: $W = r_o - r_i$ (m)
- Height loss: $h = Rr\tan(\alpha)$ (m)
- Spiral height: $H = n * u$ (m)
- Mainstream distance: $L(r) = Rr/\cos(\alpha)$ (m)

Where

R: angular distance in the mainstream direction from the spiral inlet

r: is the radial distance from the centerline axis

r_o: outer trough radii

r_i: inner radii

n: number of turns

Figure 7 depicts these parameters in a spiral concentrator

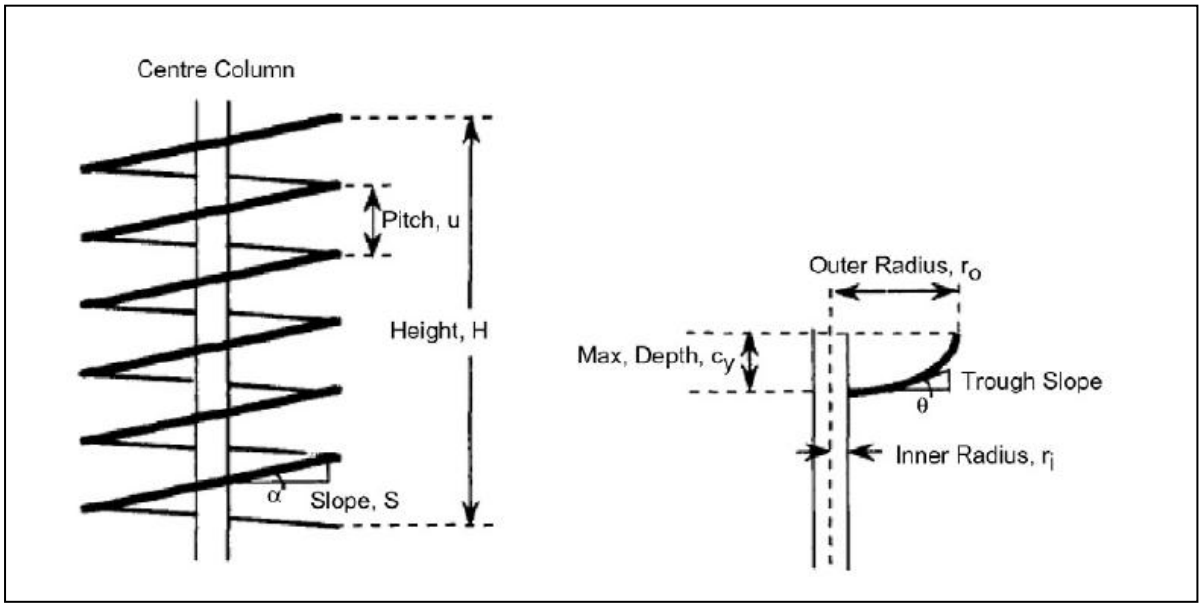

Figure 7: Parameters of the spiral geometry (Doheim et al, 2013)

The main process design parameters for a spiral concentrator include the pulp/slurry density, pulp feed flow-rate, splitter positions, particle density and size.

2.8.2. Spiral Mechanism

A spiral concentrator is a flowing film gravity concentrator, which has the combined actions of the gravity and hydrodynamic forces due to the flowing circulating film (Bayat et al, 2012). During spiraling, the pulp is subjected to centrifugal forces that cause the water and the lighter particles that are suspended to report to the outer area. This is so until the force is in equilibrium with the gravitational force (Bayat et al, 2012). As the velocity of the pulp decreases, the bottom layer has less centrifugal force and therefore follows the trough profile towards the center. This transports the heavier metals inwards to the bottom while the upper mass of water flows simultaneously outwards carrying the lighter particles (Davies et al, 1991).

The process parameters that influence the spiral performance are the feed flow rate, feed pulp density, feed particle size distribution and splitter position (Bayat et al, 2012). Generally when feed flow increases, the performance of the spiral decreases. This is the same with high density. As the splitter position becomes wider, the concentration recovery increases but the grade decreases (Falconer, 2003).

The five main principal forces acting on the particles are gravity, centrifugal, hydrodynamic drag, lift and friction forces. The equations for these forces are given below and are shown in Figure 8 (Kapur et al, 1998).

Gravity force is given by

$$F_g = \frac{\pi}{6} d^3 g(\sigma - \rho) \qquad \text{Equation 2.27}$$

Where d is the diameter of the particle, g is the gravitation constant σ is the density of the particles and ρ is the density of the fluid. The particles are assumed to be spherical.

Centrifugal force is given by

$$F_c = \frac{\pi}{6}\frac{d^3 v^2 (\theta - \rho)}{r}$$ Equation 2.28

Where v is the velocity of the particle, θ is the local slope angle in the transverse direction and r is the radial distance for the centerline

Drag force is given by

$$F_d = \frac{\pi}{4}\rho g h d^2 \sin\alpha$$ Equation 2.29

Where α is the slope angle and h is the depth of the flow

Lift force is given by

$$F_L = k_1 F_d$$ Equation 2.30

Where k_1 is the experimentally determined constant

Friction forces is given by

$$F_F = F_n \tan\theta$$ Equation 2.31

Where Fn is the normal components of all forces acting on a particle

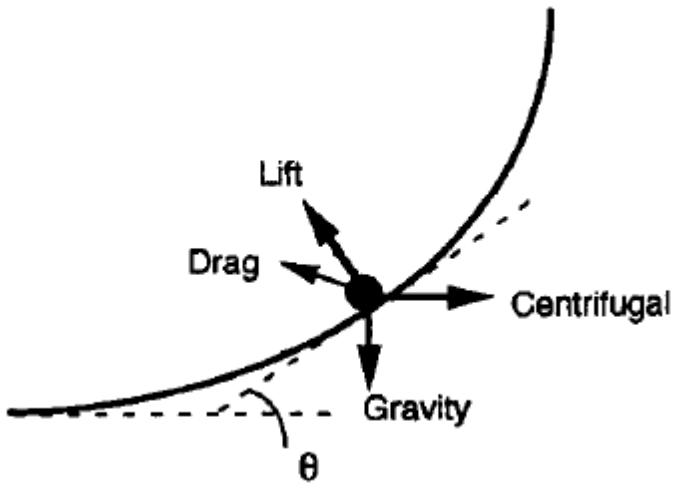

Figure 8: Forces acting on the particles in a spiral (Kapur et al, 1998)

2.8.3. Modeling the spiral

A couple of models have been developed in literature for performance of gravity concentrators. When modeling a one stage spiral operation a following simple mass balance envelope can be considered;

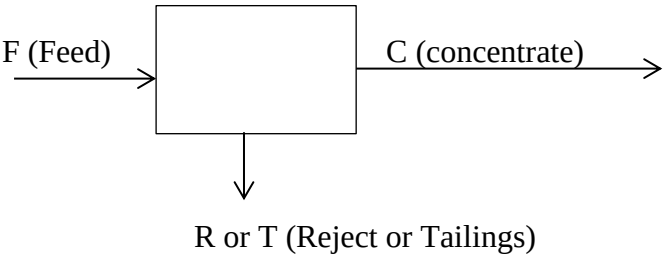

Figure 9: Schematic diagram of a single stage spiral operation

Where F – is the feed, C – is the mass that reports to the concentrate, R or T – is the mass that reports to the tailings

C/F = P is a dimensionless probability function which selects where the particles will report to, based on their physical properties (Kohmuench, 2000)

A number of useful empirical functions to describe an ideal classification have been developed and these have been adapted to describe classification in gravity concentrators. Some common classification functions are given below;

Rosin-Rammler $e(d_p) = 1 - e^{(-0.693x^{\lambda})}$ Equation 2.32

Exponential Sum $e(dp) = \frac{e^{x\lambda} - 1}{e^{x\lambda} + e^{\lambda} - 2}$ Equation 2.33

Logistic $e(dp) = \frac{1}{1 + x^{\lambda}}$ Equation 2.34

Where $x=d_{particle}/d_{50}$ and λ represents the sharpness of classifications (King, 2000). These functions can also be written with respect to density as shown below (Rao, 2004).

Rao, 2004 mentions that the models developed by Lynch and Rao (1968) and Plitt (1971) are for single particles. These models are seen below

$$Y = \frac{\exp(\alpha x) - 1}{\exp(\alpha x) + \exp(\alpha) - 2} \qquad \text{Equation 2.35}$$

$$Y = 1 - \exp\left[-x^m \ln(2)\right] \qquad \text{Equation 2.36}$$

where Y is fraction of feed reporting to sink, $x = \rho / \rho_{50}$ is ratio of particle density ρ to cut density ρ_{50} , and parameters α and m reveal the sharpness of separation.

Klima and Luckie (1989) developed a model extending from the two above to represent a bi-attribute system i.e. a system that takes into account the particle density and size. The model is represented by the following equation;

$$Y = \frac{100}{1 + \exp\left[\ln(Y^{-1} - 1) + 1.099(\rho_p - \rho)/(k.d^n)\right]} \qquad \text{Equation 2.37}$$

The model parameters k and n are estimated using a least square fit.

Rao et al. (2003) also proposed a model for bi-attribures of size & density partitioning of particles by allowing for a random walk on settling particles that are resisted by the drifting fluid within the separator as;

$$Y = 50\left[1 - erf\left(Ad^c(\rho - \rho_p) - B\right)\right] \qquad \text{Equation 2.38}$$

Where - A,B and c are model parameters

Rao, 2004 further developed a model which represents a partition surface in terms of particle size as well as density. The model is based on the equation 2.35 above. By constraining the entire partition curve to pass through the pivot coordinates and eliminating cut-density point then,

$$Y = 100\left(1 - \exp\left(-\left(\ln\left(\frac{1}{1 - Y_p}\right)\right)\left(\frac{\rho}{\rho_p}\right)^m\right)\right) \qquad \text{Equation 2.39}$$

Where Yp and ρp, are model parameters based on the operating conditions and if the operating conditions remain constant so does these parameters. m can be written as a power law to incorporate the effect of particle sizes as follows;

$$m = p.d^{q}$$ Equation 2.40

Parameters p and q determines the sharpness of the partition surface. Then the equation becomes

$$Y = 100\left(1 - \exp\left(-\left(\ln\left(\frac{1}{1-Y_p}\right)\right)\left(\frac{\rho}{\rho_p}\right)^{pd^{q}}\right)\right)$$ Equation 2.41

Where Yp, p and q are model parameters based on the operating conditions. Once these parameters are known, then the probability function can be determined.

3. Materials and Methods

The following sections discuss the materials and the experimental methods that were used to conduct laboratory scale experiments that generated the data utilized in this present work. The experiments were done by 2 fellow students who were involved in the earlier components of the research.

3.1. The High Carbon Ferro-Chrome Slag

A 2 ton sample of high carbon ferrochrome slag from a HCFeCr Smelter operation in Zimbabwe was received by the School of Chemical & Metallurgical Engineering. The slag particles measured 80% passing 25mm in size and of a head grade given in Table 4 below;

Table 4: Head grade of the as received slag sample

Component	**SiO_2 (%)**	**Al_2O_3 (%)**	**MnO (%)**	**MgO (%)**	**Fe (%)**	**Cr (%)**
Head Grade	32.31%	19.71%	0.31%	29.06%	2.9%	11.59%

3.2. Batch Milling Test-work

The original slag sample was crushed to 100% passing 13.5mm using a lab scale jaw crusher from which the following 5 monosized fractions were generated for further milling test-work; Class 1 (-13.2 + 9.5) mm, Class 2 (- 9.5 + 5.6) mm, Class 3 (-5.6 + 4) mm, Class 4 (-4 + 2.8) mm and Class 5 (- 2.8 + 1.18) mm.

Wet ball milling experiments were carried out using a 0.3 × 0.28 m variable speed laboratory ball mill. During the milling tests, one parameter was varied at a time while keeping other parameters constant at their reference values (Anac et al, 1994). Table 5 presents the range and the reference values of the main milling parameters that were studied.

Table 5: A range and reference values of main milling parameters used in the experiments

Milling Parameters	**Range**	**Reference values**
Mill speed,%	60 – 90	85
Ball filling, %	Fixed	30
Ball sizes, mm	Fixed	30
Ball density, kg/m^3	Fixed	4716 kg/m^3
Powder filling, %	60 – 100	80
Water content, %	20 – 40	30

Where;

Mill speed - is defined as % of critical speed N_{crit}.

Ball filling - is defined as the volume % of the mill filled with grinding balls.

Powder filling - is defined as % of void volume between balls filled by particles to be milled.

Water content - is defined as the mass of water divided by the mass of water and solids inside the mill.

3.2.1. Categories of batch milling experiments performed on the mono-sized classes

The milling experiments performed on each size class were divided into three categories. One category led to the determination of breakage functions while the other category led to establishment of selection functions and the last set determined PSD at different milling conditions.

3.2.1.1. Determination of breakage functions

Wet milling tests were performed on each of the size fractions prepared. The sample and the balls were loaded to the mill and each particle size class was milled for at most 30 seconds to minimize secondary breakage. Each milled sample was filtered using a pressure filter and then placed in the oven for drying. Dry sieve analysis was done to get the mass retained in smaller particle size classes; the smallest sieve used in the sieve nest was 75 microns. The retained mass is used to find the mass or fraction broken into smaller particle size classes when a certain particle size class is milled i.e. the retained masses give the breakage function of particle size class that is being milled. The cumulative breakage function, B_{ij} was obtained from the following expression;

$$B_{ij} = \sum_{k=i+1}^{n} b_{kj}$$

3.2.1.2. Determination of selection functions

Each particle size class was wet milled for 1, 2, 3, 4, up to 8 minutes, varying one parameter at a time. After each time interval, wet screening was performed to determine the retained mass of each particle size class that was milled. The plots of the retained mass or fractions of each particle size class versus milling time (first-order plots) were done. For the plots to be linear, the axis for milling time has a linear scale while the axis for the retained fraction has a logarithm scale. The slope of each graph gives the selection function or breakage rate of each particle size class.

3.2.1.3. Wet ball milling for measuring assay for each size class

A homogenous sub-sample was milled for a duration of 30 minutes and the mill product wet screened through a stack of standard lab screens with sizes ranging 13.2 mm to 0.006 mm. The material retained on each screen was dried and sent for XRF analysis to determine the chemical composition.

3.2.1.4. Wet ball milling of particle size distribution

Various predetermined feed size distributions were milled for a period of time under certain milling conditions. Sieve analysis was performed to get the resultant size distributions. Wet milling of the different particle size distributions was done three times at different grinding times and operating conditions. The experimental product size distribution was then compared with the one predicted by the rate-mass balance method.

3.3. Single stage spiral testwork

A 98 kg ferro-chrome slag sample with the particle size distribution shown in Table 6 and Figure 10 was used as the feed to the spiral concentration unit. The spiral used was a 5 turn spiral equipped with a feeding manifold, a collection sump with a mixer and a pump, the spiral had 2 adjustable stream sampling splitters which were used to collect timed samples of concentrates and tailings after steady state. The feed sample was made into slurry of 25% solids and 75% water by weight. The slurry was fed to the spiral for the rougher stage at a

feed rate of 2 t/hr solid dry basis. After steady state was deemed to have been attained the samples were collected, dried and prepared for analysis.

Table 6: Particle size distribution of the feed to the spiral

Sieve Size range (mm)	Nominal Sieve Size (mm)	Individual Weight retained (g)	Individual % weight retained (%)	Cumulative % Passing	Cumulative % Retained
-1	1	0	0	100	
-1 + 0.710	0.710	224.4	22.4	77.6	22.4
-0.710 +0.500	0.500	198.3	19.8	57.8	42.2
-0.500 + 0.355	0.355	198.7	19.8	38.0	62.0
-0.355+0.212	0.212	93.2	9.3	28.7	71.3
-0.212+0.150	0.150	107.2	10.7	18.0	82.0
-0.150+0.106	0.106	61.9	6.2	11.8	88.2
-0.106+0.075	0.075	62.9	6.3	5.5	94.5
-0.075+0.053	0.053	19.4	1.9	3.6	96.4
-0.053+0.038	0.038	25.6	2.6	1.0	99.0
-0.038	0.000	10.1	1.0	0.0	100.0

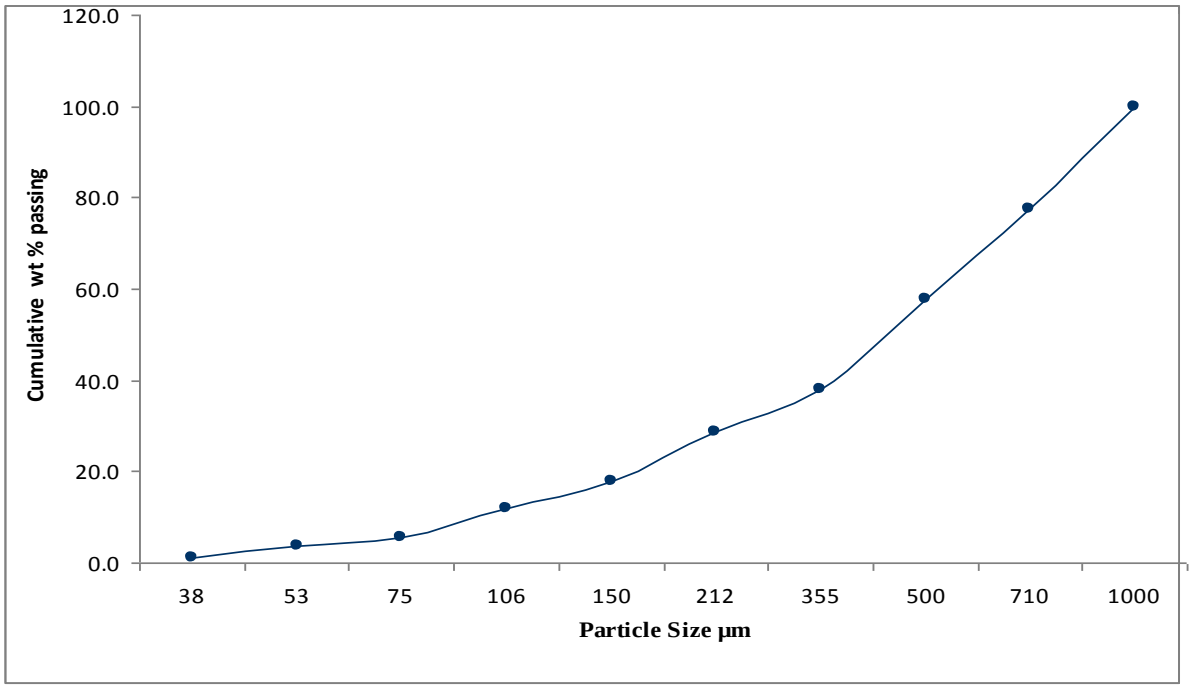

Figure 10: Particle size distribution of the feed to the spiral

The feed to the spiral was such that it maximised the particles size of about 1 mm that showed the best liberation and minimized the – 75 microns particles that generally form slimes and are known to have a negative effect on the spiral performance.

4. Results and Discussion

4.1. Assay by size

The Table 7 gives the XRF results showing the chemical analysis for different size classes of particles. The data in Table 7 is represented graphically in Figure 11 in respect to each size fraction content of Cr and Fe which are the main elements of interest in specifying the grade of ferro-chrome slag. From Figure 11 it can be seen that the particle content of both Cr and Fe behave similarly for the different size classes. The content of the metals increases as the grind gets finer i.e. from the top size -13.2 + 9.5 mm and reaches a maximum at particle size around +/_ 1mm. The metal content then decreases slightly for the particles < 1mm. The reason could be that the free grains of the ferrochrome alloy that were trapped in the slag during the smelting process were probably droplets that are in that size region. To maximise the recovery of the metal from the slag one would have to mill the material in such a way that particles in this size range are maximised.

Table 7: Assays for each size class

Assays for each size class						
Component	**SiO_2 (%)**	**Al_2O_3 (%)**	**MnO (%)**	**MgO (%)**	**Fe (%)**	**Cr (%)**
Head Grade	32.31%	19.71%	0.31%	29.06%	2.90%	11.59%
-13.2+9.5mm	35.80%	20.10%	0.32%	28.50%	2.10%	6.90%
-9.50 +5.6mm	34.70%	19.80%	0.36%	27.90%	2.10%	7.60%
-5.6+4 mm	33.90%	19.40%	0.34%	28.20%	2.30%	8.80%
-4+2.8 mm	33.40%	18.20%	0.38%	27.90%	3.50%	10.10%
-2.8+1.18 mm	32.80%	17.80%	0.30%	27.80%	4.10%	11.20%
-1.18+0.85 mm	29.70%	17.50%	0.35%	24.30%	5.30%	13.60%
-0.8+0.6 mm	29.80%	18.10%	0.34%	25.10%	5.20%	13.10%
-0.6+0.15 mm	31.28%	18.10%	0.30%	27.82%	3.14%	11.81%
-0.15+0.075 mm	31.30%	18.30%	0.33%	29.30%	2.53%	10.65%
-0.075+0.006mm	31.50%	18.60%	0.32%	29.80%	2.49%	10.38%
-0.006+0mm	31.50%	18.70%	0.31%	30.20%	2.38%	10.32%

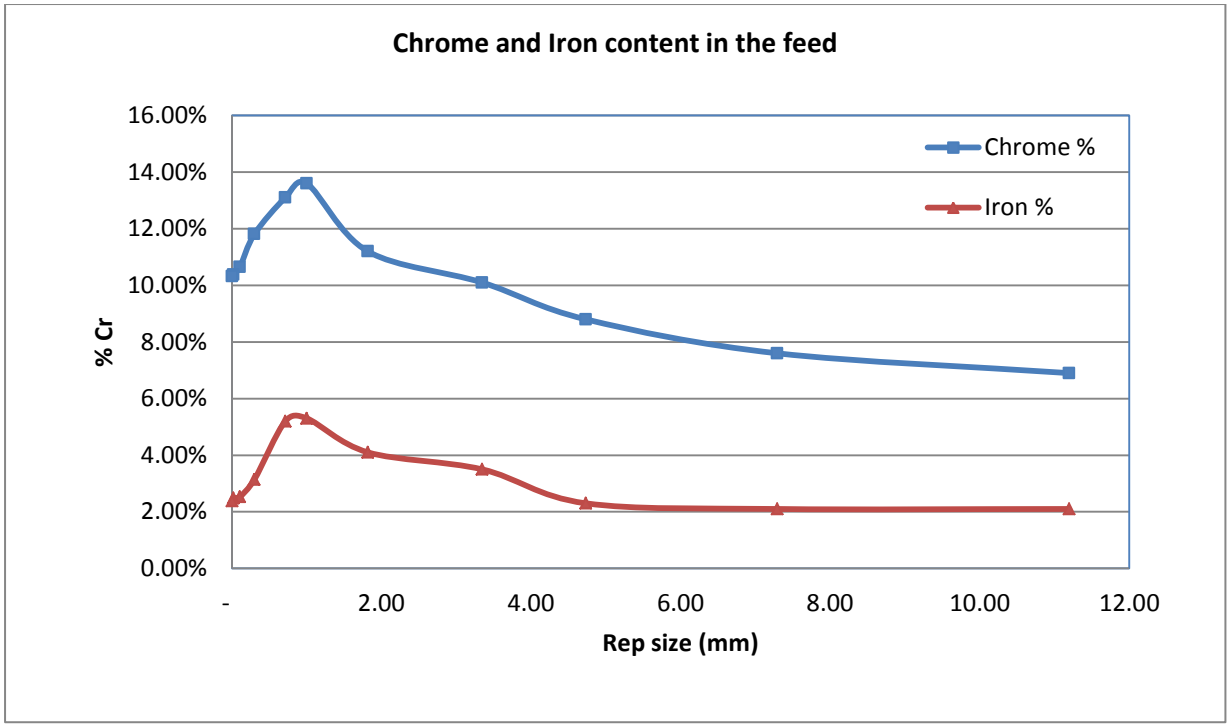

Figure 11: Chrome and iron content in the feed

4.2. Modeling Approach

The following sections discuss the results obtained from the modeling work. The models/equations used were coded into excel spreadsheet. The selection and breakage functions were obtained directly from milling experimental tests performed on the high carbon ferro-chrome slag. The measured selection and breakage functions were imported into the relevant models and the minimization of sum of squared errors (SOS) function solver in excel was used to calculate model parameters using the experimental data to come up with predictive models. With breakage and selection functions established, a population balance batch milling model was used to simulate particle size distribution of mill product for different operating conditions to arrive at the conditions that give the most favorable spiral feed.

4.2.1 Estimating selection function using first order plots

Selection functions were estimated using equation 2.2. Figure 12, Figure 13 and Figure 14 show the first order plots for different mill conditions. Table 8 shows the estimated selection functions for all particles size fractions and mill conditions.

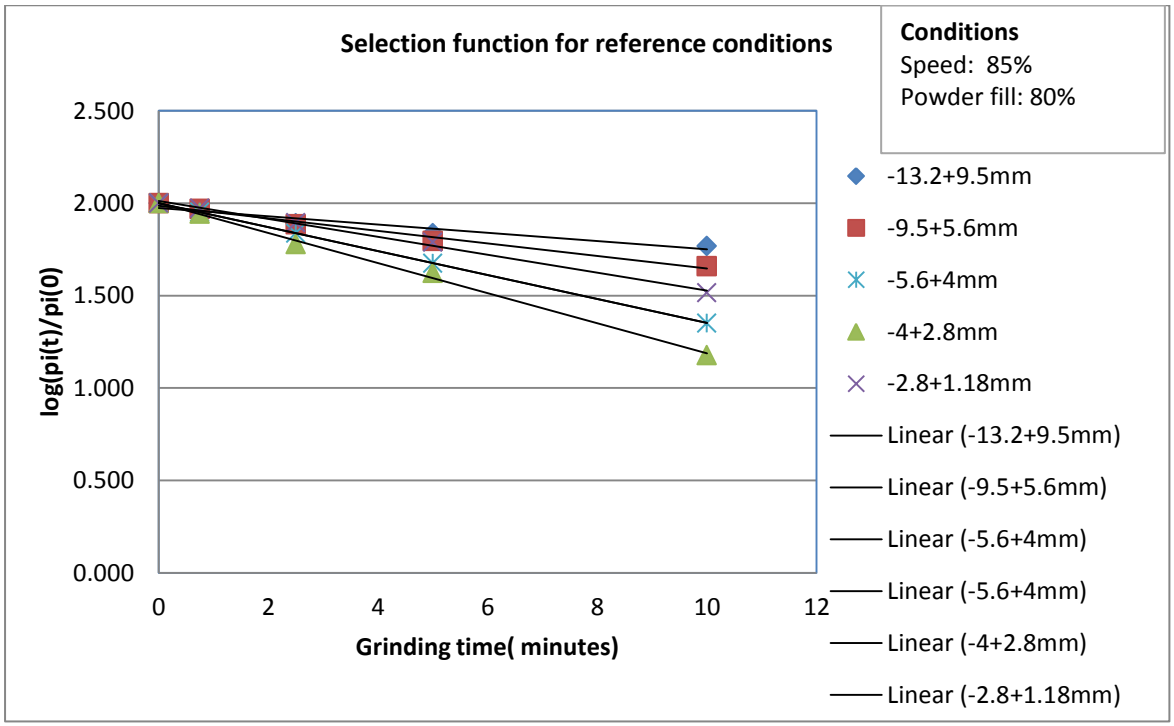

Figure 12: First order plots for reference conditions

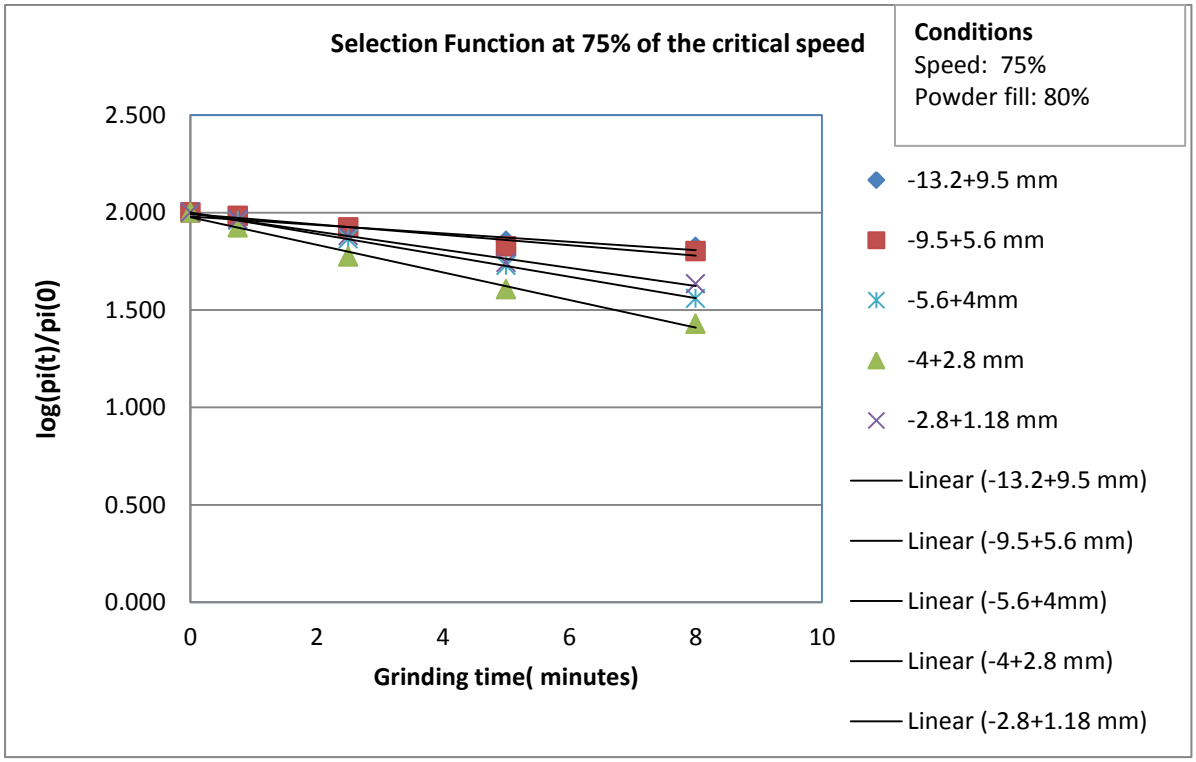

Figure 13: First order plots for 75% critical speed

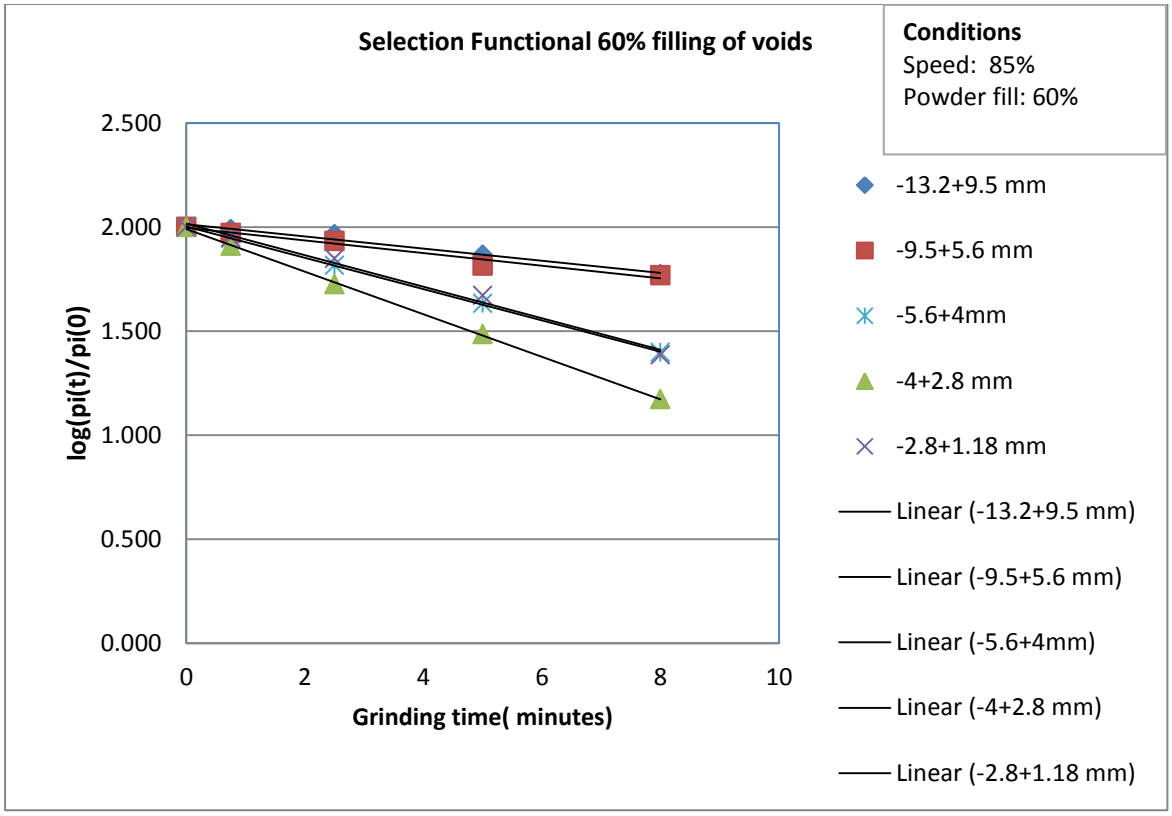

Figure 14: First order plots 60% powder filling

Table 8: Experimental selection function from first order plots

Selection Function (min^{-1})			
Size Fractions	**Reference Conditions**	**75% Critical Speed**	**60% Powder Filling**
-13.2+9.5 mm	0.051	0.050	0.067
-9.5+5.6 mm	0.078	0.061	0.070
-5.6+4.0 mm	0.149	0.127	0.173
-4.0+2.8 mm	0.188	0.163	0.236
-2.8+ 1.18 mm	0.112	0.107	0.174

The results, in general, show that the selection function of each size class, regardless of the milling conditions, increases in value from the size class -13.2 + 9.5 mm to size class – 4.0 + 2.8 mm and then decreases sharply for the lower size class of -2.8 + 1.18 mm.

Mill speed can affect the grinding efficiency and this can be seen by the difference in the selection functions at different milling conditions. The Selection functions at reference conditions and 60% powder filling are higher than at 75% critical speed. This is because the

critical speed at reference conditions and at 60% powder filling is 85%, which is higher than 75%. At higher mill speed the faster the breakage of the particles to the undersizes therefore the higher the selection function within the speed rage explored. The peak in the selection function can be due to the change from cascading to cataracting pattern (Deniz, 2004).

The amount of powder in the mill affects the output of the mill and this can be seen by the varying selection function when the powder fill is changed. The selection function is higher at 60% powder filling compared to the reference conditions and the 75% critical speed. This is because powder filling for reference conditions and the 75% critical speed are both higher at 80%. As powder fill is increased, the mass hold-up of the mill increases. This then leads to poor nipping collisions and therefore decreasing the breakage rates. The lower powder fill produces finer products compared with higher powder filling which produces coarser products from the mill.

4.2.1.1 Effect of particle sizes on selection function

The Austin model shown in equation 2.4 is an empirical correlation that is generally used to calculate selection functions for different size classes. This model has parameters a, α, μ and Λ that require determination as they are material specific. The experimental selection functions with their respective size fractions were applied to the model and the minimisation of sum of squared errors method applied to estimate the parameters. These parameters are given in Table 9

Table 9: Parameters from Austin model

Parameters			
Constants	**Reference Conditions**	**75% Critical Speed**	**60% Powder Filling**
a	0.001	0.001	0.002
α	4.9	4.9	4.9
Λ	6.2	6.2	6.2
μ	3.2	3.1	2.9

From Table 9 it can be seen that the Austin model parameters do not vary much over the different conditions used in the experimental work hence an average of these 3 values was considered to fairly represent each parameter.

The Austin model, with all its parameters specified, was used to calculate the model selection functions for each size class and Table 10 gives the results of the model calculations.

Table 10: Selection function calculated from the Austin model

Selection Function (min-1)			
Size Fractions	**Reference Conditions**	**75% Critical Speed**	**60% Powder Filling**
-13.2+9.5 mm	0.051	0.043	0.058
-9.5+5.6 mm	0.078	0.065	0.088
-5.6+4.0 mm	0.149	0.125	0.169
-4.0+2.8 mm	0.188	0.163	0.230
-2.8+ 1.18 mm	0.112	0.107	0.176

Figure 15, Figure 16 and Figure 17 compare the predicted selection functions using the Austin model and the experimental selection functions calculated using the first order plots at different conditions. There is good prediction of the selection functions demonstrating the validity of the parameter estimation method applied.

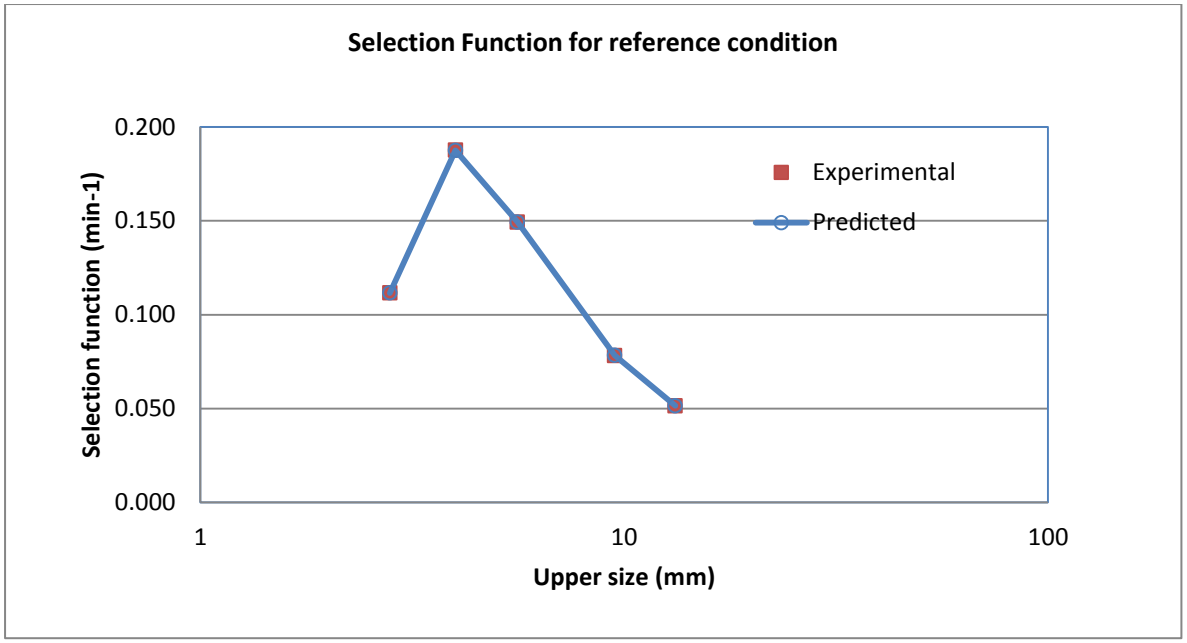

Figure 15: Comparison between experimental and calculated selection functions for reference condition

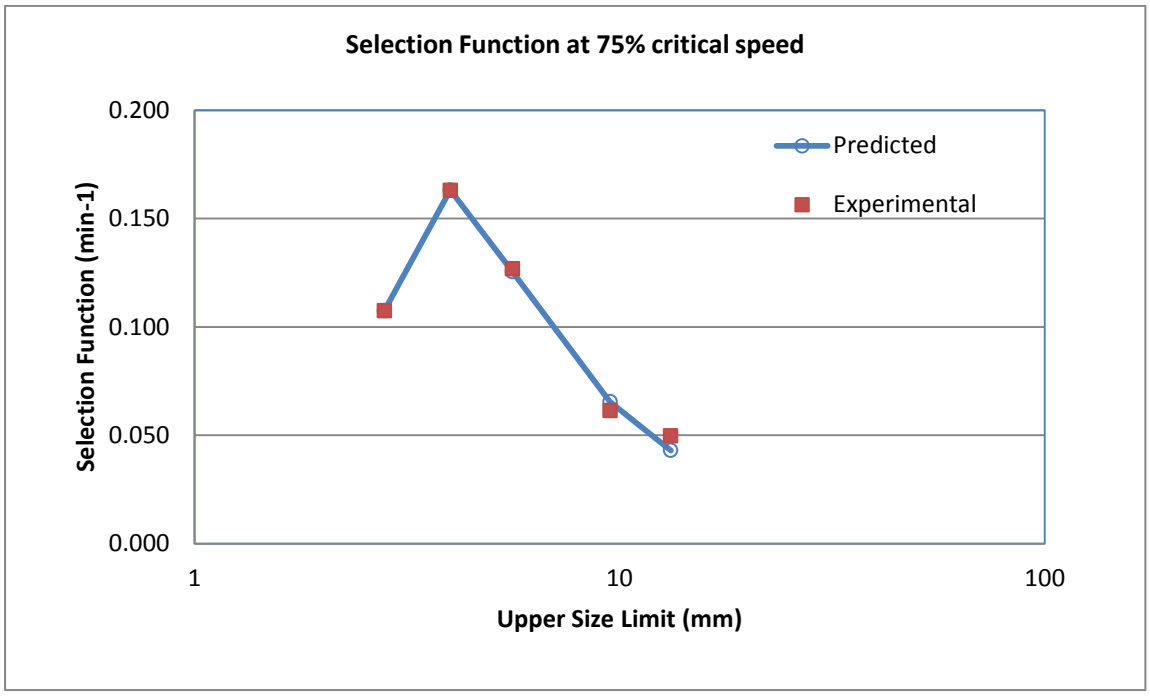

Figure 16: Comparison between experimental and calculated selection functions for 75% critical speed

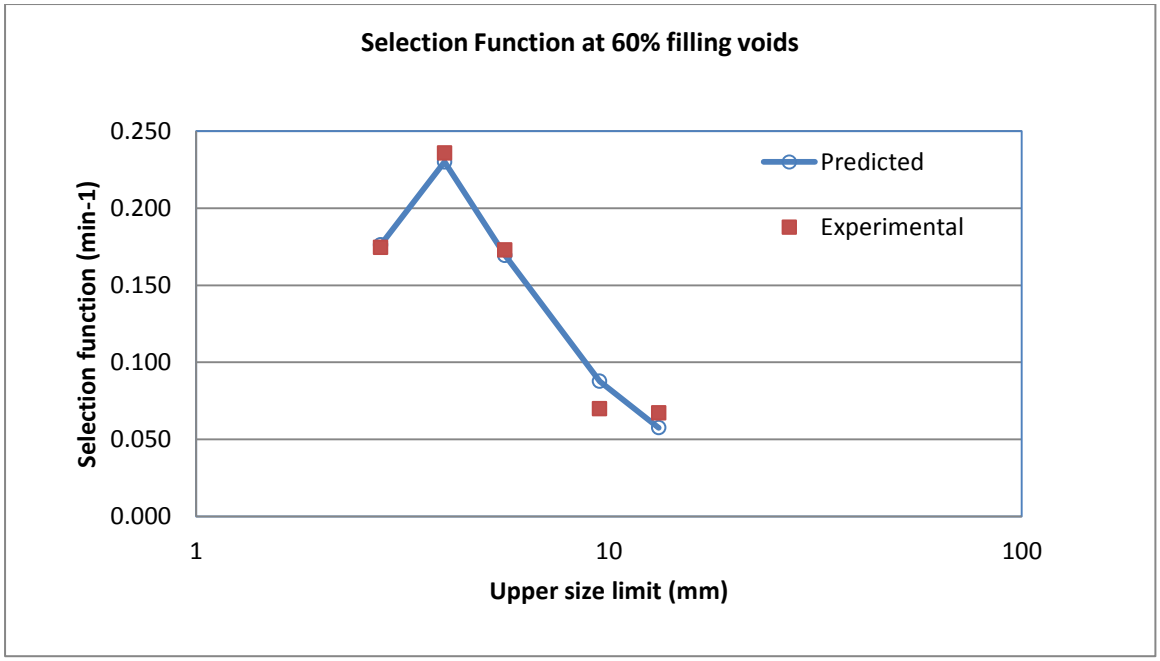

Figure 17: Comparison between experimental and calculated selection functions for 60% powder filling

From the above Figure 15, 16 & 17, it can be concluded that the predicted selection functions fit well with the selection functions determined from first order plots of the experimental results over the conditions that were tested.

4.2.1.2 Selection function at different conditions

This section aims to use the modified Austin model shown in Equation 2.5 to predict selection functions at the different conditions used. Multipliers C_1 to C_5 were to be tested. C_1, C_2 and C_3 were kept at 1 as ball diameter (d) and mill diameter (D) were not changed. Only C_4 and C_5 were tested. Table 11 shows the parameters that best fit the different milling conditions and selection function using equation 2.5. Table 12 shows selection functions calculated from Modified Austin Model. The plots comparing the predicted selection functions with the experimental selection functions can be seen in Figure 18.

Table 11: Parameters of the modified Austin Model

Parameters			
Constants	**Reference conditions**	**75% Critical Speed**	**60% Powder Filling**
Multipliers	1.000	1.026	1.302
α	4.9	4.9	4.9
Λ	6.2	6.2	6.2
a	0.001	0.001	0.002
μ	3.2	3.1	2.9

Table 12: Selection Function calculated from Modified Austin Model

Selection Function (min-1)			
Size Fractions	**Reference Conditions**	**75% Critical Speed**	**60% Powder Filling**
-13.2+9.5 mm	0.051	0.043	0.058
-9.5+5.6 mm	0.078	0.065	0.088
-5.6+4.0 mm	0.149	0.125	0.169
-4.0+2.8 mm	0.188	0.163	0.230
-2.8+ 1.18 mm	0.112	0.107	0.176

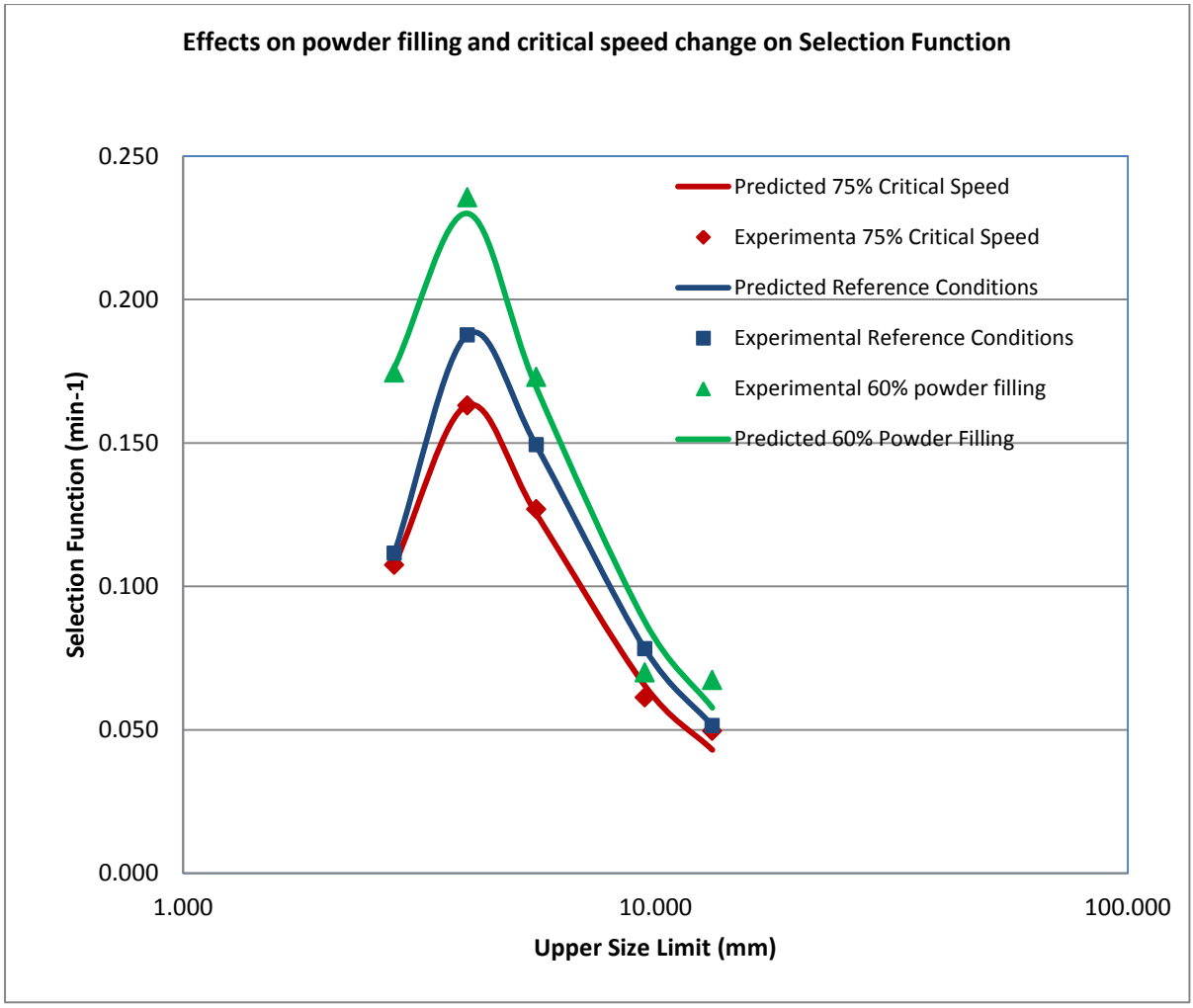

Figure 18: Comparison between experimental and calculated selection function for all milling conditions

From the Figure 18, the effect of powder filling and change in critical speed can be clearly seen. The lower the powder filling, the higher the selection function of each particle size class and the lower the critical speed the lower the selection function, (Chimwani et al, 2014, Deniz, 2004) this was found to be consistent with literature.

Average values for the model parameters that will be used in the simulation using the Austin model are as seen in Table 13

Table 13: Average selection function model parameters

Parameters	Values
a	0.001
α	4.9
Λ	6.2
μ	3.1

4.3. Breakage Function

Experimental breakage functions were calculated using the BII method given in equation 18 and the Austin model given in equation 2.19. Figure 19, Figure 20 and Figure 21 show the cumulative breakage functions for the first 4 size classes for all the milling conditions.

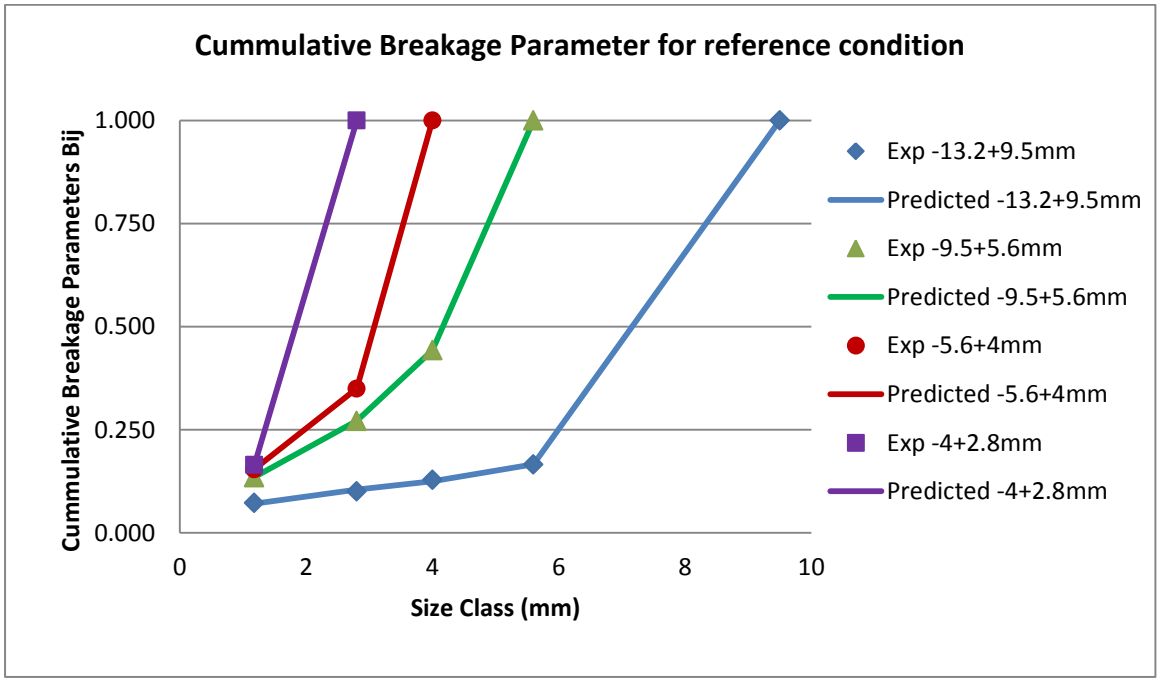

Figure 19: Cumulative breakage function for reference conditions

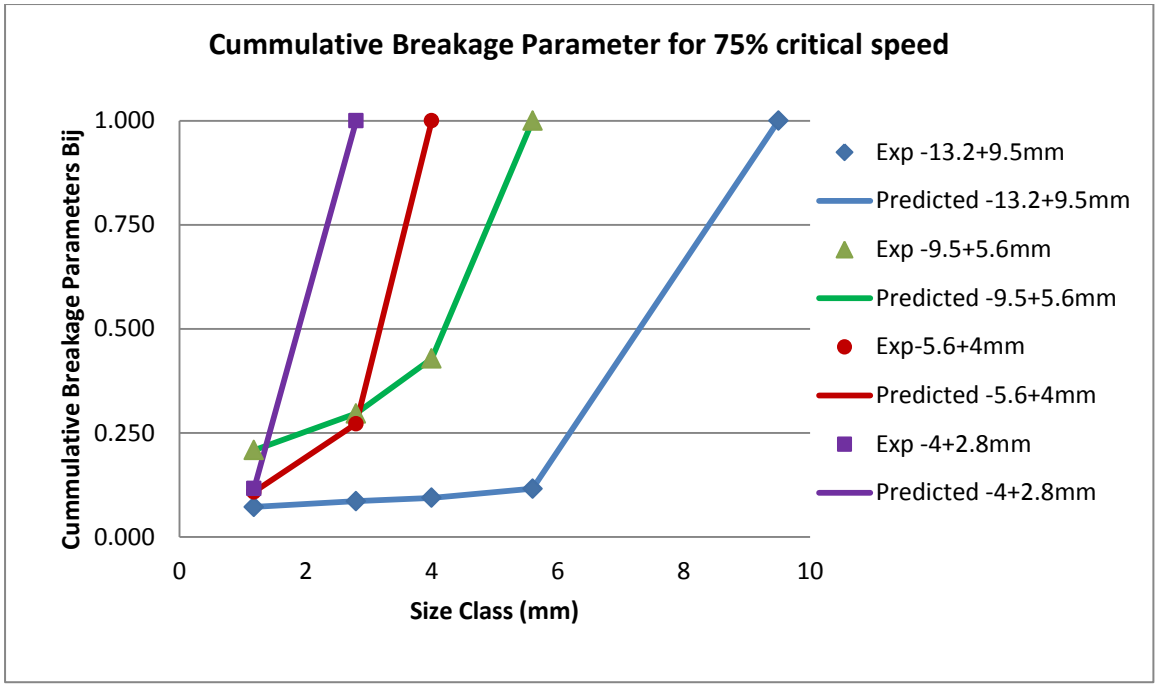

Figure 20: Cumulative breakage function for 75% critical speed

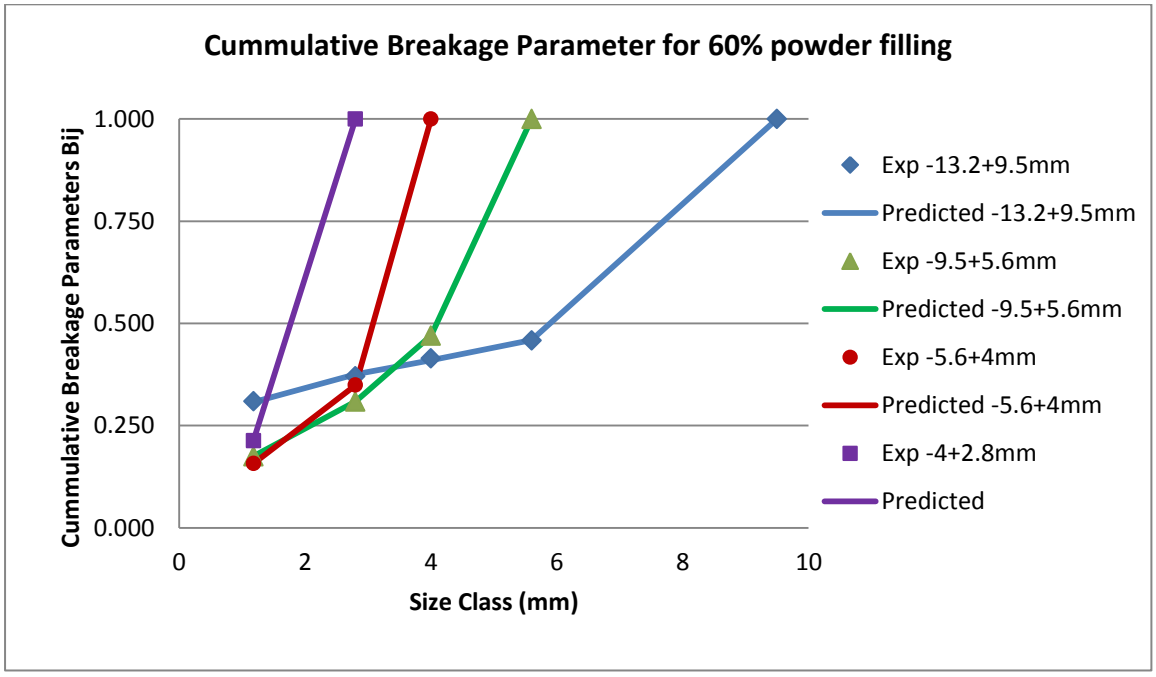

Figure 21: Cumulative breakage function for 60% powder filling

From Figure 19, Figure 20 and Figure 21, one can see that the predicted cumulative breakage functions fit the experimental cumulative breakage functions well. The average parameter values that are proposed for use in the simulations are given in Table 14.

Table 14: Average breakage function model parameters

Parameters	Values
φ_j	0.3
γ	0.6
β	5.7

This is in line with suggestion from Chimwani et al, (2013), who suggested than the β parameter is characteristic of the material used and it is generally above 2.5, γ is material dependant and the values are typically found to be above 0.6, while φ_j represents the fractions of fines that are produced from the mill and this parameter also depends on the material and ranges from 0 to 1.

4.4. Particle size distribution

The population balance equation given in equation 2.21 and the model constants/parameters that were calculated above were used to simulate the particle size distribution at different conditions. These were compared to the experimental data. Figure 22, Figure 23 and Figure 24 show the predicted values and the experimental values.

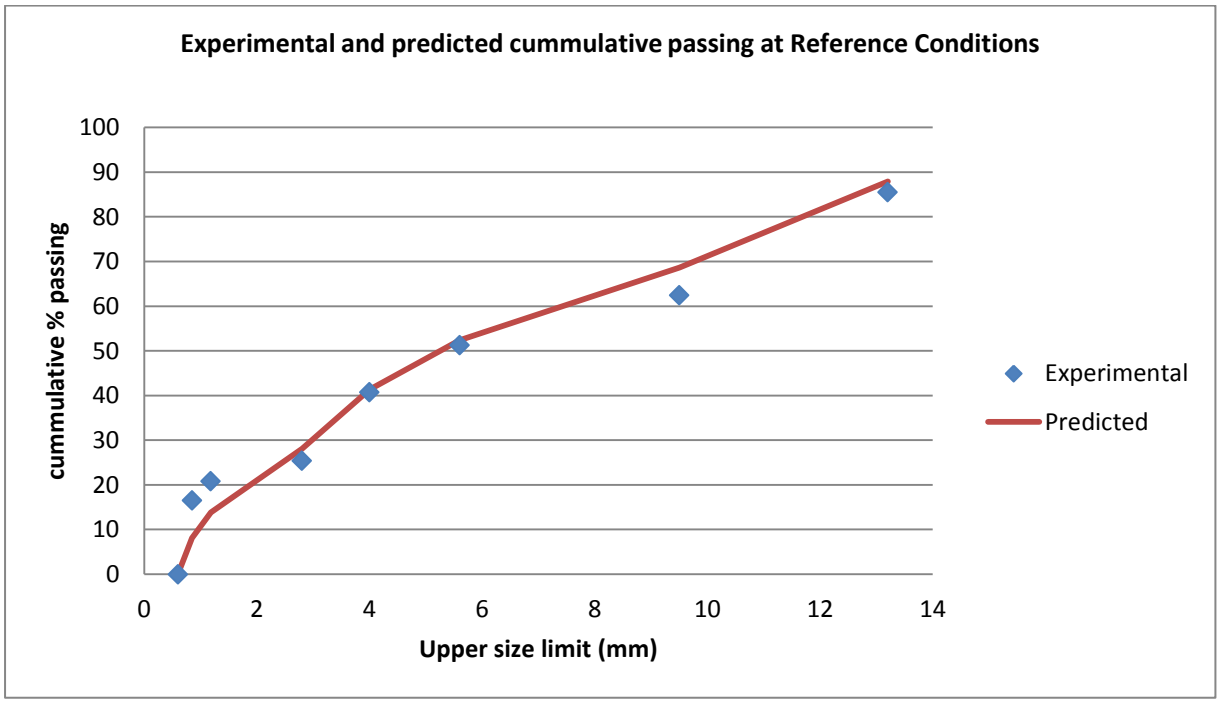

Figure 22: Experimental and predicted cumulative passing at Reference Conditions at 85% Critical Speed and 80% Powder Filling

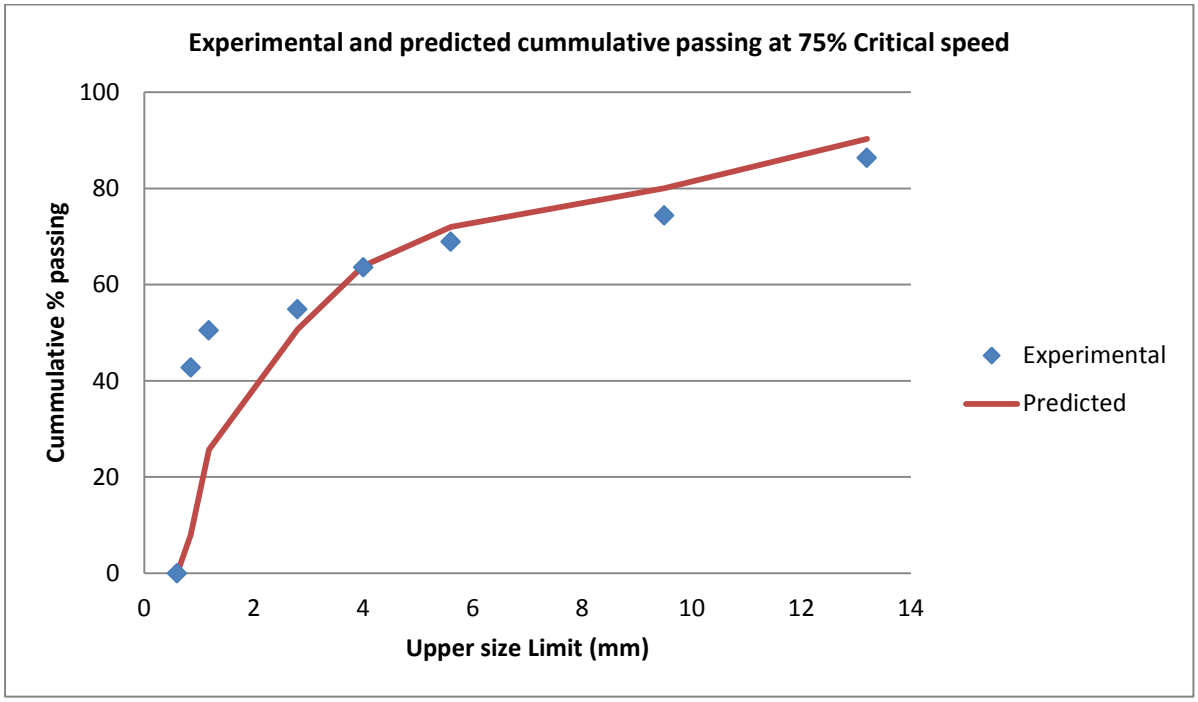

Figure 23: Experimental and predicted cumulative passing at 75% critical speed

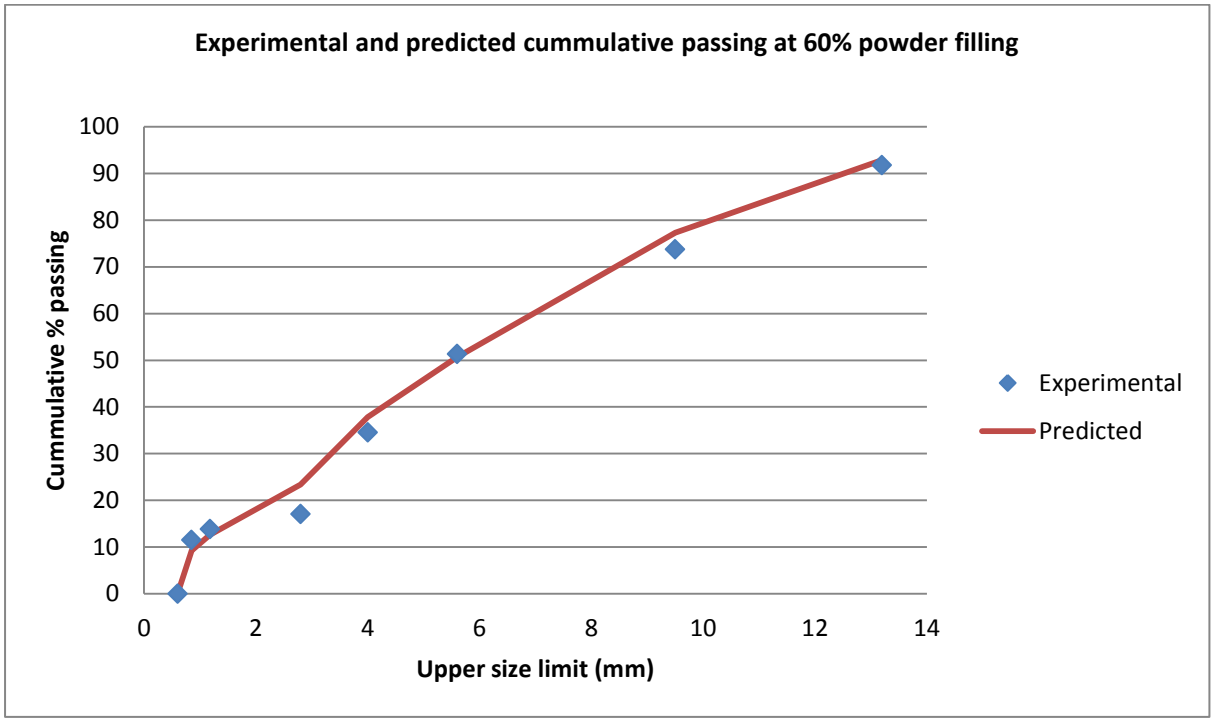

Figure 24: Experimental and predicted cumulative passing at 60% powder filling

From Figure 22, 23and 24 it can be seen that the predicted product size distribution fits the experimental data reasonably well. The greatest deviation is seen when varying critical speed especially at sizes below 4mm.

4.5. Model optimization

The population balance model was used to predict the best possible milling operating conditions that maximizes the generation of particles between -1.18 mm and 0.075 mm. This size range showed optimum liberation in the size by assay tests. This particle size range is also ideal for spiral concentration according to literature where particles less than 0.075 mm are normally removed by de-sliming to improve the efficiency of the spiral process.

The selection and breakage functions obtained earlier were used and the conditions of the mill were varied to get different mill product. These conditions were estimated using solver to maximise the products in the recommended size classes. The best mill conditions are shown in Table 15 below where there are compared to the reference conditions. Figure 25 shows the cumulative passing of the ball mill with the optimal conditions as well as the reference conditions. The table with these size classes can be seen in the Appendix A3.

Table 15: Optimal operating conditions

Operating conditions	**Optimal**	**Reference**
Powder filling,	60%	80%
Fraction of Critical speed,	80%	85%
Ball Size	30	30
Ball filling	20%	30%

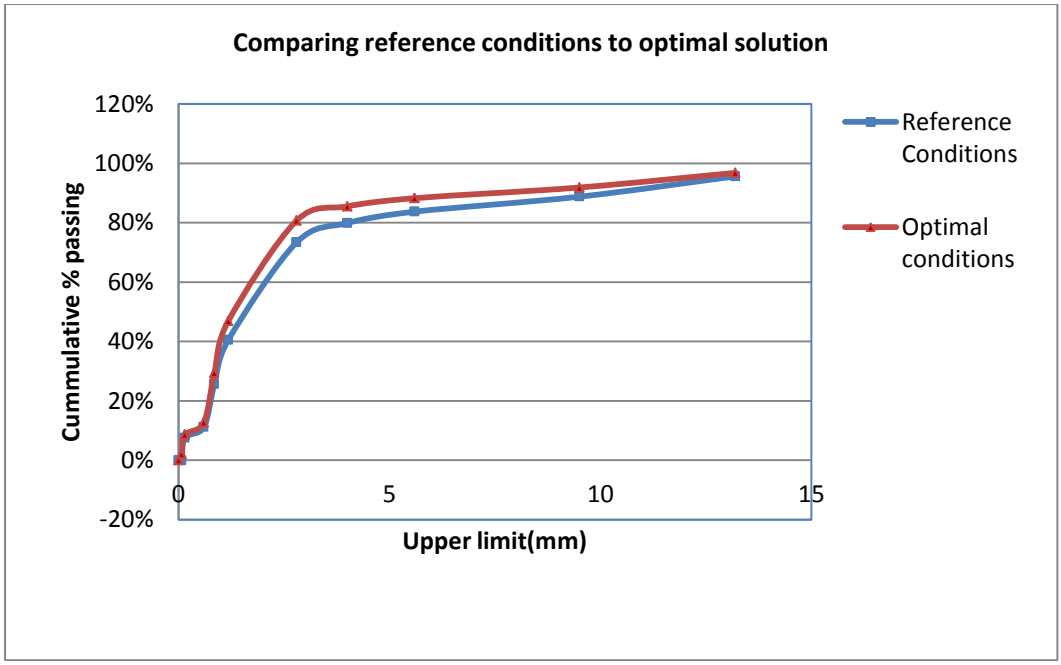

Figure 25: Comparing optimal conditions to reference conditions

The mill product size distribution derived from the optimal milling conditions showed a marginal improvement on the reference conditions. This may be due to the fact that the initial reference conditions, which were based on literature, were already the recommended conditions for milling this kind of material, therefore already close to ideal conditions.

4.6. Spiral Modeling

Single stage (rougher) spiral experiments outline in Section 3.3 of the Materials and Methods chapter were done to measure single stage recovery.

Table 16 shows the overall results from the one stage spiral experiment. The Cr content of the feed, concentrates and tailings was considered here since ferro-chrome products are generally classified on the basis of their Cr content or units.

Table 16: Results of the overall mass balance for the one stage spiral experiment

Unit	Feed	Concentrates	Tailings
Mass (kg)	98.00	40.20	57.80
Chrome (%)	11.70	17.21	7.87
Chrome (kg)	11.47	6.92	4.55

From the results given in Table 16 the overall yield of the single spiraling stage is given by;

$$Y_{tot} = \frac{C}{F} = \frac{40.20}{98.00} = 0.41$$ Equation 4.1

Overall yield shows the percentage of the feed that reports to the concentrates.

4.6.1. Model parameter estimation

The prediction of the recovery of a single spiraling stage was attempted using 2 models; the first model used is represented by equation 2.35 by Lynch and Rao (1968) and also shown below. This model assumes that the particle size distribution of the feed to the spiral is narrow and closely controlled hence is does not influence the separation taking place in the spiral i.e. it suggests that the only variable affecting separation is particle density.

$$Y = \frac{\exp(\alpha x) - 1}{\exp(\alpha x) + \exp(\alpha) - 2}$$ Equation 4.2

$$Y_{tot} = \sum Y_i = \sum \frac{\exp(\alpha x_i)}{\exp(\alpha x_i) + \exp(\alpha) - 2}$$ Equation 4.3

$$Y_{tot} = \sum Y_i = \sum \frac{\exp(\alpha \frac{\rho_{p_i}}{\rho_{50}})}{\exp(\alpha \frac{\rho_{pi}}{\rho_{50}}) + \exp(\alpha) - 2}$$ Equation 4.4

Where i – is the i^{th} particle in the feed size distribution

Y_{tot} is total recovery that was measured in the experiments and it represents a cumulative total of the different particle size classes recovered from the feed to the concentrates. The density of each particle size in the feed size distribution was individually calculated on the basis of the chemical composition of each particle which is given in Table 7. The densities of the pure compounds making up the particles were found from literature and used to calculate the approximate particle densities using weighted averages. The spreadsheet for the density calculation is given in Appendix A4.

Knowing Y_{tot} and the ρ_{pi} , the model was used to estimate cut off density ρ_{50} and parameter α using the sum of squared errors. ρ_{50} represents the density of a particle that has a 50 % chance of either reporting to the concentrate or the tailings. Due to limited information, it was assumed that 50% of the chrome is liberated and the rest is locked with the other minerals like iron silicate minerals (Tripathy et al, 2012).

The second model used is represented by equation 2.41 by Rao (2004) and this model assumes that the particle size distribution of the feed to the spiral as well as the particle density affect the separation during spiraling. The same liberation assumption was also made for this model. The model bt Rao (2004) is given as;

$$Y = 100\left(1-\exp\left(-\left(\ln\left(\frac{1}{1-Y_p}\right)\right)\left(\frac{\rho}{\rho_p}\right)^{pd^q}\right)\right) \qquad \text{Equation 4.5}$$

Which can also be written as;

$$Y_{tot} = \sum Y_i = \sum 100\left(1-\exp\left(-\left(\ln\left(\frac{1}{1-Y_p}\right)\right)\left(\frac{\rho}{\rho_{pi}}\right)^{pd_i^q}\right)\right) \qquad \text{Equation 4.6}$$

The sum of squared errors was also used to estimate the parameters of the bi-attribute model where the particles are now defined by both their size d_{pi} and density ρ_{pi}.

Table 17 and Table 18 show the parameters of each respective model calculated using the sum of squared errors.

Table 17: Model parameters for first model (density only) – Lynch & Rao. (1968)

Model Parameters	
Constants	**Values**
ρ_{50}	4,195
α	3.83

Table 18: Model parameters for second model (density and particle sizes) – Rao. (2004)

Model Parameters	
Constants	**Values**
Y_p	0.32
ρ	3,322
p	42.64
q	0.30

Substituting the model parameters back into the respective model equations gives the following;

Single attribute density model: Lynch & Rao. (1968)

$$Y = \frac{\exp\left(3.83\frac{\rho_{pi}}{4.195}\right)}{\exp\left(3.83\frac{\rho_{pi}}{4.195}\right) + \exp(3.83) - 2} \qquad \text{Equation 4.7}$$

Figure 26 gives the partition curve of Equation 4.7 which shows the chance or probability that a particle of a particular density has to either report to the concentrates or tailings during spiral concentration i.e. a particle of density 6000 kg/m^3 has a 80 % chance of reporting to the concentrate according to the model.

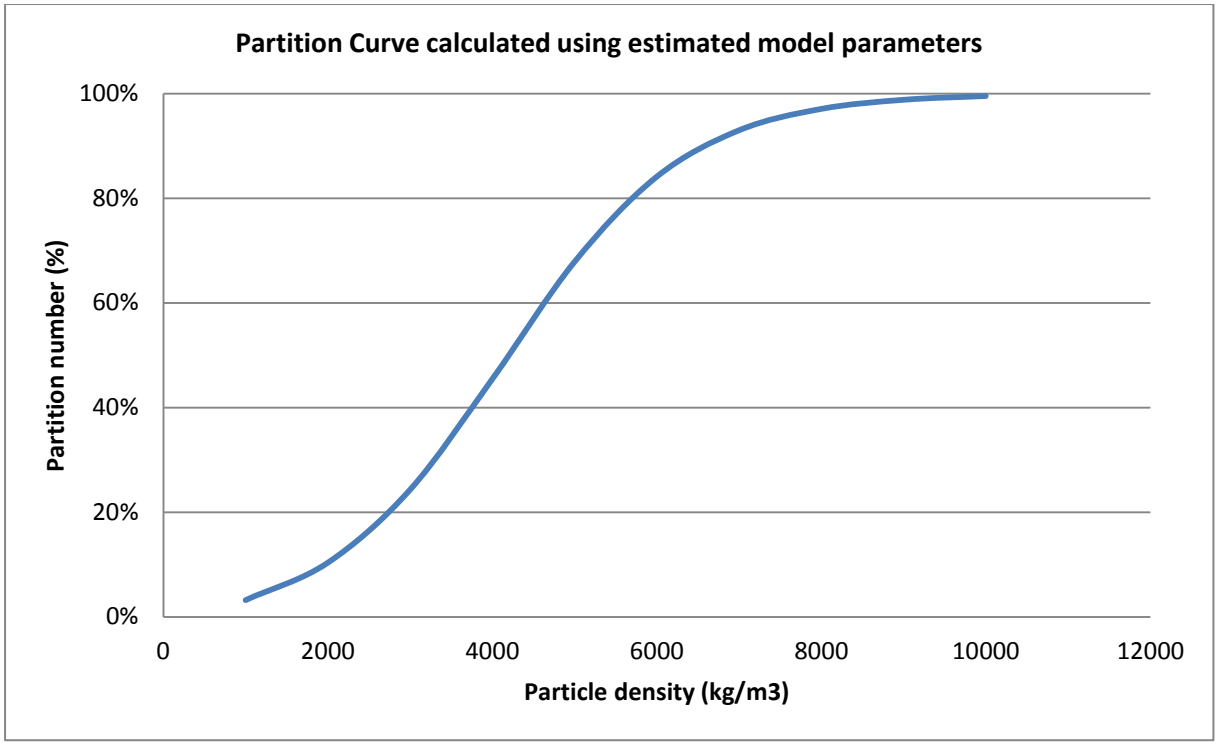

Figure 26: Partition Curve calculated using estimated model parameters

Bi-attribute density & size model: Rao. (2004)

$$Y = 100\left(1-\exp\left(-\left(\ln\left(\frac{1}{1-0.32}\right)\right)\left(\frac{3.322}{\rho_{pi}}\right)^{42.64 d_{pi}^{0.3}}\right)\right)$$

Equation 4.8

Figure 26 shows the partition curve of Equation 4.8, the bi-attribute model, where partition is a function of both particle size and density.

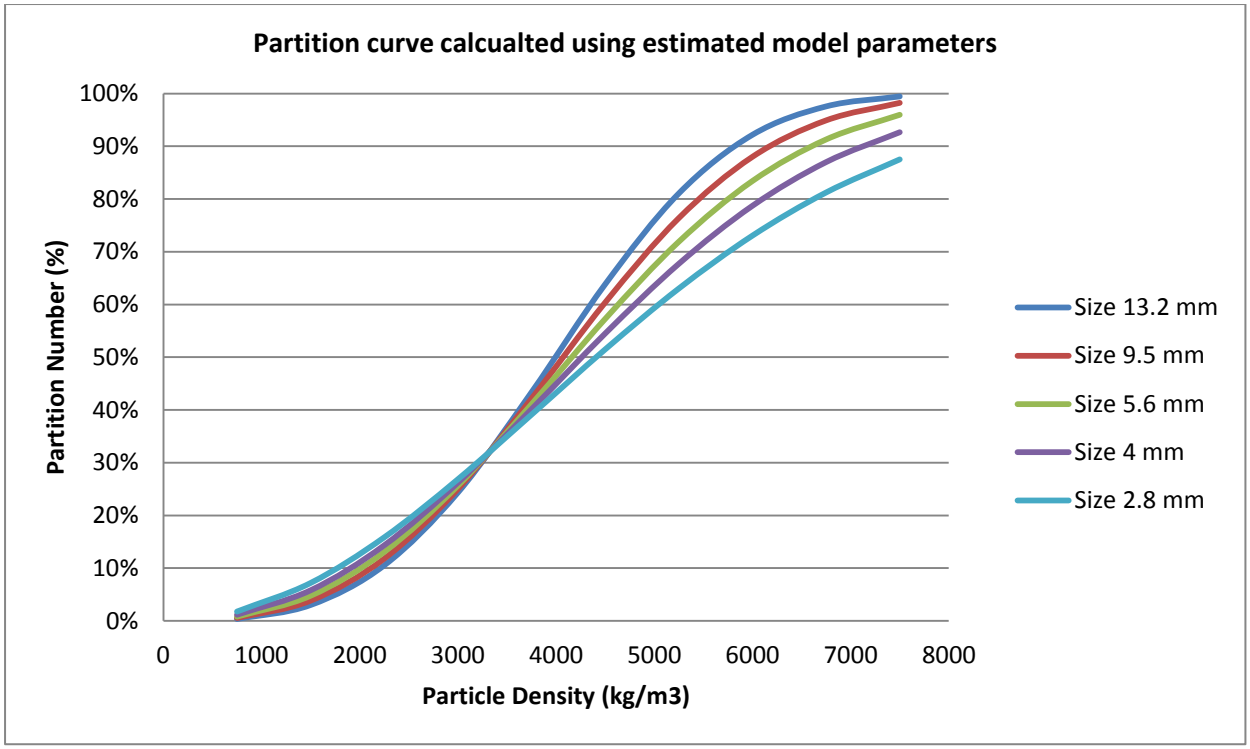

Figure 27: Partition Curve calculated using estimated model parameters

The two recovery models described above were then used to predict the grade and the recovery of the concentrates obtained from a single stage rougher spiraling experiments. The predicted grades and recoveries were then compared to those which were measured experimentally to establish which of the 2 models gives a superior simulation of the experimental observations.

Table 19 shows data and variables that were used to calculate the concentrate recovery and grade based on Lynch and Rao (1968) model

Table 19: Data for recovery and calculation using Lynch & Rao model (1968)

Size Range (mm)	Rep Size drep (mm)	Particle Density	% Cr	% In Feed	Mass in 2 Ton Feed	Y model Lynch & Rao	Mass in Cons	Mass of Cr in Cons
+ 1.000					-		-	-
-1.000 + 0. 710	0.843	3.732	11	22.4	0.45	39.29%	0.18	0.03
-0.710 + 0.500	0.596	3.937	13	19.8	0.40	43.99%	0.17	0.03
-0.500 + 0.355	0.421	3.807	12	19.8	0.40	41.00%	0.16	0.03
-0.355 + 0.212	0.274	3.807	12	9.3	0.19	41.00%	0.08	0.01
-0.212 + 0.150	0.178	3.807	12	10.7	0.21	41.00%	0.09	0.02
-0.150 + 0.106	0.126	3.773	11	6.2	0.12	40.22%	0.05	0.01
-0.106 + 0.075	0.089	3.773	11	6.3	0.13	40.22%	0.05	0.01
-0.075 + 0.053	0.063	3.738	10	1.9	0.04	39.43%	0.02	0.00
-0.053 + 0.038	0.045	3.738	10	2.6	0.05	39.43%	0.02	0.00
-0.038	0.019	3.722	10	1.0	0.02	39.08%	0.01	0.00
					2.00		0.82	0.16

Yield = Sum (mass in cons)/Sum (mass in feed)

= 41%

Grade of concentrates = Sum (mass of Cr in cons)/Sum (mass in cons)

= 18.91%

Table 20: Data for recovery and concentrate grade calculation using Rao model (2004)

Size Range (mm)	Rep Size drep (mm)	Particle Density	% Cr	% In Feed	Mass in 2 Ton Feed	Y model Rao	Mass in Cons	Mass of Cr in Cons
+ 1.000					-		-	-
-1.000 + 0. 710	0.843	3.732	11	22.4	0.45	41.71%	0.19	0.03
-0.710 + 0.500	0.596	3.937	13	19.8	0.40	45.15%	0.18	0.03
-0.500 + 0.355	0.421	3.807	12	19.8	0.40	41.23%	0.16	0.03
-0.355 + 0.212	0.274	3.807	12	9.3	0.19	40.06%	0.07	0.01
-0.212 + 0.150	0.178	3.807	12	10.7	0.21	39.03%	0.08	0.01
-0.150 + 0.106	0.126	3.773	11	6.2	0.12	37.87%	0.05	0.01
-0.106 + 0.075	0.089	3.773	11	6.3	0.13	37.27%	0.05	0.01
-0.075 + 0.053	0.063	3.738	10	1.9	0.04	36.38%	0.01	0.00
-0.053 + 0.038	0.045	3.738	10	2.6	0.05	35.94%	0.02	0.00
-0.038	0.019	3.722	10	1.0	0.02	34.93%	0.01	0.00
					2.00		0.82	0.15

Yield = Sum (mass in cons)/Sum (mass in feed)

= 41%

Grade of concentrates = Sum (mass of Cr in cons)/Sum (mass in cons)

= 18.11%

Table 21: Comparison of the experimental and model recoveries

Comparing model and experimental data			
	Experiment	Model 1 Lynch & Rao (1968) (density only)	Model 2 Rao (2004) (density and particle size)
Feed Cr%	11.70%	11.70%	11.70%
Grade/Concentrate Cr %	17.21%	18.91%	18.11%
Recovery	41%	41%	41%

From Table 21 it can be seen that the concentrate grade prediction from the bi-attribute model i.e. the model that factors the contribution of both the particle size and density, is closer to the

experimental value than the model that considers density only. The difference is not too material though, as the classes which comprises of larger sizes have smaller mass fractions.

4.6.2. Modeling of the spiral using ball mill product distribution

The same procedure used above was utilized to calculate the concentrate grade and recoveries from a single stage spiral process that is fed with a simulated feed size distribution. The simulated feed particle size distribution used is the one which was found to be the optimum distribution from the milling modeling.

Table 22: Comparison of the experimental and model recoveries using optimized ball mill product

Comparing model and experimental data			
	Experiment	Model 1 Lynch & Rao (1968) (density only)	Model 2 Rao (2004) (density and particle size)
Feed Cr%	11.70%	11.92%	11.92%
Concentrate Cr %	17.21%	18.13%	17.67%
Recovery	41%	42%	45%

The recovery obtained in the cases of both models for the concentration of the ideal feed size distribution is more than that obtained from the experiments. This indicates that the simulated particle size distribution is superior in richness/liberation of particles which are submitted to the spiral for concentration. The grade also increases showing that a more liberated feed is being processed.

4.4 Discussion

The high carbon ferrochrome slag received from the slag dump was analysed chemically and the analysis showed that the slag contained about 11.6 % Cr , 2.9 % Fe, 32% SiO_2, 19.7% Al_2O_3 and 29 % MgO as head grade. This metal content is considered to be high enough for metal recovery to be carried out profitably. Size by assay test were also carried out to investigate the degree of liberation that can be achieved by milling, the results showed that the metal content increased as the grind became fine and that particles around 1 μm were the most well liberated as shown in Table 7. The reason could be that the free grains of the ferrochrome alloy that were trapped in the slag during the smelting process were probably

droplets that are in that size region. To maximise the recovery of the metal from the slag one would have to mill the material in such a way that particles in this size range are maximised.

In order to model the milling operation the key milling parameters namely the selection function and the breakage function were determined experimentally. The results for the selection function, shown in Table 8, show that the selection function of each size class, regardless of the milling conditions, increases in value from the size class -13.2 + 9.5 mm to size class – 4.0 + 2.8 mm and then decreases sharply for the lower size class of -2.8 + 1.18 mm, indicating that, for this material, the size class – 4.0 + 2.8 mm breaks up much more easily than other size classes. The results in Table 8 also show that when powder filling is reduced i.e. from 80% to 60% the breakage rate of each size class is increased. This suggests that when the amount of material in the mill is reduced the particles have a higher chance of making impact collisions with the media balls causing more breakage while at higher powder fill the relative motion between the powder and the balls is reduced. A decrease in the mill speed from 0.85 N_{crit} to 0.75 N_{crit} resulted in a drop in the breakage rate of the material showing that there is less energy at lower speed such that the breakage mechanism shifts from being largely due to impact to attrition (Deniz, 2004). The selection function data were fitted to the Austin model to generate the model parameters. The Austin model, with all parameters estimated, was then used to predict the selection functions at a variety of milling conditions. The selection functions together with the breakage functions shown in Figure 19, Figure 20 and Figure 21, were used in conjuction with the population balance model to predict the particle size distribution of the mill product. The results in Figure 22, Figure 23 and Figure 24 show the experimental mill product size distribution at different milling conditions and the corresponding model predictions, a good agreement between the model and the experiments is seen. This suggests that the parameters were reasonably well estimated and that the population balance is a credible model for milling. The model was used to simulate the best milling conditions that will give the maximum amount of the most liberated particle size i.e. mill product that is largely +/- 1 mm. It was found that milling conditions of; 60% powder fill, 80 Ncrit mill speed & 20 % ball fill were the most ideal to mill the material in such a way that it gives the best liberated product, these milling conditions are not too different from the reference conditions of 80% powder fill, 85 Ncrit mill speed & 30 % ball fill which were recommended from the literature as good conditions for milling this kind of material.

A spiral concentrator was proposed in this study as a concentration or separation method to separate the ferro-chrome alloy from the slag in mill product in order to upgrade the concentration of the Cr & Fe to a saleable grade of ferrochrome concentrate. The saleable or marketable grade has been shown to be above 44% by Murthy et al, 2011.The attraction of the spiral was that it can handle finely milled material more efficiently than other gravity concentration methods. Suitable spiral models i.e by Lynch & Rao (1968) & Rao (2004) were evaluated and their parameters estimated from the given experimental data. The parameters for the Lynch & Rao (1968) model were found to be; ρ_{50}= 4,195 kg/m^3 and α= 3.83 and those for the Rao (2004) model were estimated as Y_p= 0.32, p= 42.64, q= 0.3 and ρp = 3,322 kg/m^3. The model by Lynch and Rao (1968) considers that separation of particles in a spiral happens only because of the density difference of the particles and the other developed by Rao (2004) takes into account both particle size and density. The two recovery models were used to predict the grade and the recovery of the concentrates obtained from single stage rougher spiraling experiments. Both models reasonably predicted the experimental grade (17.21% Cr in concentrate) and yield of 41% obtained from a single stage rougher spiral test though the Rao (2004) model was superior in its prediction. Even though this is the case, the grade from the model was lower than the sealable grade using the one stage spiral technique.

5. Conclusions and recommendations

This project involved the modeling of a mill and spiral concentrator as a proposed process to recover the high carbon ferrochrome alloy content of the slag. The work covered modeling of the mill and the spiral concentrator units, experimental data from earlier studies were used to estimate the model parameters. The parameters were imported into the model functions to come up with predictive functions. The predictions from the models were compared with experimental data to establish their validity.

This section of the report gives answers to the research questions that were set out at the beginning of the research.

What are the selection and breakage functions and parameters for this high carbon ferrochrome slag?

The breakage functions and the selection functions for different size classes and different conditions were determined from the experiments and used to estimate the parameters of the selection function Austin model by use of sum of squared errors. The parameters for the Austin model were calculated as follows; a= 0.001, α= 4.9, Λ= 6.2 and μ= 3.1 and φi= 0.3, γ=0.6 and β= 5.7 respectively. The parameters predicted were fed to a batch milling population balance model to predict the mill particle size distribution at different conditions. The model prediction was reasonably good leading to the conclusion that the parameters were estimated accurately.

What are the effects of particle sizes, change in critical speed and powder filling on the breakage rates?

The effect of particle size on the selection function for the milling of high carbon ferrochrome slag was established. The selection function increased with decreasing particle size fraction from size fraction -13.2 + 9.5, -9.5 + 5.6 mm, -5.6 + 4.0 and -4.0 + 2.8 mm and then marginally increased for the size fraction -2.8 + 1.18mm. This trend was observed for all the conditions tested i.e. different powder filling and different critical speeds.

The effect of powder filling and change in critical speed on the selection function was also determined. The lower the powder filling the higher the selection function and the lower the

critical speed the lower the selection function. This observation was found to be in line with literature review (Chimwani et al, 2014, Deniz, 2004). This means that for higher selection of a given particle size range a higher the speed and lower the powder filling is preferred.

What particle size distribution is obtained using the batch milling population balance model?

The simulated particle size distribution showed a good agreement with the experimental measurements with the greatest deviation seen when varying critical speed especially at sizes below 4mm. The milling conditions were also varied in the model to maximize the production of particles in the size range – 1.18 mm and 0.075mm mill product because this size range showed superior liberation in the assay by size tests. The optimum condition were found to be; powder filling of 60%, fraction of critical speed of 80%, ball size of 30mm and ball filling of 20%.

The overall mill product size distribution derived from the optimal milling conditions showed a measurable improvement on that from the reference conditions.

What are the predictions of the spiral concentration models?

Suitable spiral models i.e by Lynch & Rao (1968) & Rao (2004) were evaluated and their parameters estimated from the given experimental data. The parameters for the Lynch & Rao (1968) model were found to be; ρ_{50}= 4,195 kg/m^3 and α= 3.83 and those for the Rao (2004) model were estimated as Y_p= 0.32, p= 42.64, q= 0.3 and ρp = 3,322 kg/m^3. The model by Lynch and Rao (1968) considers that separation of particles in a spiral happens only because of the density difference of the particles and the other developed by Rao (2004) takes into account both particle size and density. The two recovery models were used to predict the grade and the recovery of the concentrates obtained from single stage rougher spiraling experiments. Both models reasonably predicted the experimental grade (17.21% Cr in concentrate) and yield of 41% obtained from a single stage rougher spiral test though the Rao (2004) model was superior in its prediction. The grade predicted by the models was lower than the sealable grade of above 44%. This indicates that further concentration is needed to improve the grade.

In conclusion, the aims of this project were addressed as a model was developed to predict the particles size distribution from the mill at varying operating conditions. The model for the spiral concentrators was also applied and does predict the recovery to the concentrates and the chrome content.

Recommendations

Based on the status of this study when it was completed it is recommended that further work be done on developing a complete spiral circuit to upgrade or concentrate the values in the slag to saleable grade of > 44 % Cr content. In the current work only rougher spiral concentration was considered and the recovery model was tested on the basis of that first level concentration stage. The effect of pulp/slurry density, pulp feed flow-rate and splitter positions for the Spiral concentrator need to be examined as well. The milling and spiraling experiments which were done to provide the data for modeling were done separately and in the future it is recommended that a rig be built that can combine the 2 unit operation into 1 flow sheet so that variables changed in the milling can have their effect measured directly in the final product coming out of the spiral process and this would improve the modeling of the process.

6. References

Anaç S., Erglin Ş and Sönmez B., 1994, Effects of some variables on the cumulative basis kinetic model parameters in ball mill grinding, Progress in Mineral Processing technology, pp533-538.

Austin L.G., Trimarchi T., Weymont N.P., 1977, An analysis of some cases of non-first order breakage rates, Powder Technology 17 (1), pp 109 – 113

Austin L.G., Klimpel R.R., Luckie P.T., 1984, Process engineering of size reduction, SME, pp 62 – 78

Bayat O., Ay O., Unal S., 2012, Pre-concentration of chromite ores with Krebs Spiral Concentrator, Kilavuz Ltd. and Mining Engineering Department of Cumhuriyet University, pp 1-7

Chimwani N., Glasser D., Hildebrandt D., Bwalya M.M., Mulenga F.K., 2014, Scale up of batch grinding data for simulation of industrial milling of platinum group minerals ore, Minerals Engineering 63, pp 100–109

Chimwani N., Glasser D., Hildebrandt D., Metzger M.J., Mulenga F.K.,2013, Determination of the milling parameters of a platinum group minerals ore to optimize product size distribution for flotation purposes, Minerals Engineering 43–44, pp 67–78

Coulson J.M., Richardson J.F., Harke.r, J. H Backhurst J. R., 2002, Coulson and Richardson's Chemical Engineering, Volume 2, Particle technology and separation processes, pg 106

Davies, P.O.J., Goodman R.H., and Deschamps J.A., 1991, Recent Developments in Spiral Design, Construction and Application, Minerals Engineering, vol. 4, no. 3/4, pp. 437-456

Deniz V., 2004, The effect of mill speed on kinetic breakage parameters of clinker and limestone, Cement and concrete research 34, pp 1365 – 1371

Doheim M.A., Abdel Gawad A.F., Mahran G.M.A., Abu-Ali M.H., Rizk A.M., 2013, Numerical simulation of particulate-flow in spiral separators: Part I. Low solids concentration (0.3% & 3% solids), Applied Mathematical Modelling 37, pp 198–215

Erdema M., Altundogan H.S., Turan M.D, Tumenb F., 2005, Hexavalent chromium removal by ferrochromium slag, Journal of Hazardous Materials B126, pp 176–182

Falconer A., 2003, Gravity separation: old technique/new methods, Physical Separation in Science and Engineering, Vol. 12, No. 1, pp. 31–48

Holappa L., Xiao Y., 2004, Slags in ferroalloys production—review of present knowledge, The Journal of The South African Institute of Mining and Metallurgy, pp 429-438

Jadhav U.U., Hocheng , H., 2002, A review of recovery of metals from industrial waste, Journal of Achievements in Materials and Manufacturing Engineering, Volume 54, Issue 2 pp 159 - 167

Kapur P.C., Meloy T.P., 1998, Spirals observed, International Journal of Mineral Processing. 53, pp 15-28

Kapur P.C., Meloy T.P., 1999, Industrial modeling of spirals for optimal configuration and design: spiral geometry, fluid flow and forces on particles, Powder Technology 102, pp 244–252

Katubilwa F.M., Michael H. Moys M.H., Glasser D, Hildebrandt D., 2011, An attainable region analysis of the effect of ball size on milling, Powder Technology 210, pp36–46

King R.P., 2000, Modelling and simulation of mineral processing systems: Technical notes 8, Grinding, Butterworth-Heinemann, pp 8-39

Klima, M.S. and Luckie, P.T., 1989, Application of an unsteady-state pulp-partition model to dense-medium separations. Coal Preparation 6, pp 227-240.

Kohmuench J.N., 2000, Improving Efficiencies in Water-Based Separators Using Mathematical Analysis Tools, Mining and Minerals Engineering, Faculty of the Virginia Polytechnic Institute and State University, pp 1-40

Lameck, N.N.S., 2005, Effects of grinding media shapes on ball mill performance, University of the Witwatersrand, pp 1- 131

Lynch, A.J. and Rao, T.C., 1968, Studies on the operating characteristics of hydrocyclone classifiers. Indian Journal of Technology 6, pp 106-114.

Monov V., Sokolov B., Stoenchev S., 2012, Grinding in Ball Mills: Modeling and Process Control, Bulgarian Academy of Sciences, Cybernetics and Information Technologies, Volume 12, No 2, pp 51-68

Murthy Y.R., Tripathy S. K., Kumar R., 2011, Chrome ore beneficiation challenges & opportunities – A review, Minerals Engineering 24, pp 375–380

Niemelä P., Kauppi M., 2007, Production, characteristics and use of ferrochomium slags, Innovation in Ferro Alloy Industry 5, pp 171-179

Plitt, L.R., 1971, The analysis of solid-solid separations in classifiers. The Canadian Mining and Metallurgical Bulletin, pp 1-6.

Raghupathy L., Chaturvedi A., 2013, Secondary resources and recycling in developing economies, Science of the Total Environment 461–462, pp 830–834

Rao B.V., Kapur P.C., Rahul Konnur R., 2003, Modeling the size–density partition surface of dense-medium separators, International Journal of Mineral Processing 72, pp 443– 453

Rao B.V., 2004, Weibull partition surface representation for gravity concentrators, Minerals Engineering 17, pp 953–956

Shen H., Forssberg E., 2003, An overview of recovery of metals from slags, Waste Management 23, pp 933–949

Somez B., Demirel B., 2010, Determination of breakage parameters in laboratory scale ball mill and scale up of ball milling, Hacettepe Univeristy, Mining engineering department

Sripriya R., Murty Ch. V.G.K., 2005, Recovery of metal from slag/mixed metal generated in ferroalloy plants—a case study, International Journal of Mineral Processing 75, pp 123– 134

Toneva P., Peukert W., 2007, Modelling of Mills and Milling Circuits, Chapter 20, Handbook of Powder Technology, Volume 12, Elsevier B.V.

Tripathy S.K., Murthy Y.R., 2012, Modeling and optimization of spiral concentrator for separation of ultrafine chromite, Powder Technology 221, pp 387–394

Tripathy S.K., Singh V., Ramamurthy Y., 2012, Improvement in Cr:Fe Ratio of Indian Chromite Ore for Ferro Chrome Production, International Journal of Mining Engineering and Mineral Processing, 1(3): pp 101-106

Van Staden Y., Beukes J.P., van Zyl P.G., du Toit J.S., Dawson N.F., 2014, Characterization and liberation of chromium from fine ferrochrome waste materials, Minerals Engineering 56, pp 112–120

Watson B., 2013, Chromite Special Edition, KPMG, Commodity insights bulletin

Wills B. A., Napier-Munn T.J., 2006, Mineral processing technology, an introduction to the practical aspects of ore treatment and mineral recovery, Elsevier Science & Technology Books, pp 7-13, 146-182

Wood D.R., 2007, Rules of thumb in engineering practices, John Wiley & Sons, 27, pp 137 - 183

7. Appendices

7.1. Selection Function

Table A1 below shows the top mass size that was remaining after each time intervals and Table A2 shows the data that was used to plot the first order plots (Figures 12, 13 and 14 in the main report) as well as calculated selection functions.

Table A1: Mass in each class for different milling conditions

Mass in each Class					
Mass in each size at reference milling conditions (C1)					
Time min	-13.2+9.5 mm	-9.5+5.6 mm	-5.6+4 mm	-4+2.8 mm	-2.8+1.18 mm
0	4.75	4.75	4.75	4.75	4.75
0.75	4.371	4.42	4.25	4.17	4.467
2.5	3.699	3.659	3.27	2.855	3.736
5	3.272	2.974	2.25	1.991	2.92
10	2.79	2.17	1.07	0.715	1.56
Mass in each size when mill speed is 75% of the critical speed (C2)					
Time min	-13.2+9.5 mm	-9.5+5.6 mm	-5.6+4 mm	-4+2.8 mm	-2.8+1.18 mm
0	4.75	4.75	4.750	4.75	4.75
0.75	4.328	4.554	4.323	3.979	4.377
2.5	3.853	3.974	3.471	2.82	3.61
5	3.399	3.184	2.537	1.918	2.625
8	3.159	3.005	1.720	1.273	2.049
Mass in each size at 60% filling of voids with particles (C3)					
Time min	-13.2+9.5 mm	-9.5+5.6 mm	-5.6+4 mm	-4+2.8 mm	-2.8+1.18 mm
0	3.563	3.563	3.563	3.563	3.563
0.75	3.472	3.335	3.138	2.892	3.167
2.5	3.283	3.055	2.333	1.891	2.507
5	2.622	2.324	1.527	1.087	1.671
8	2.113	2.087	0.890	0.53	0.863

Table A2: Selection function calculated using first order slopes

Selection function Calculated using First order Slopes					
Log of Fraction retained in the top size at reference milling conditions					
	-13.2+9.5 mm	-9.5+5.6 mm	-5.6+4 mm	-4+2.8 mm	-2.8+1.18 mm
0	2.000	2.000	2.000	2.000	2.000
0.75	1.964	1.969	1.951	1.943	1.973
2.5	1.891	1.887	1.838	1.779	1.896
5	1.838	1.797	1.676	1.622	1.789
10	1.769	1.660	1.352	1.178	1.516
Slope	-0.022	-0.034	-0.065	-0.081	-0.048
Si	0.051	0.078	0.149	0.188	0.112
Fraction retained in the top size when mill speed is 75% of the critical speed					
	-13.2+9.5 mm	-9.5+5.6 mm	-5.6+4 mm	-4+2.8 mm	-2.8+1.18 mm
0	2.000	2.000	2.000	2.000	2.000
0.75	1.960	1.982	1.959	1.923	1.964
2.5	1.909	1.923	1.864	1.774	1.881
5	1.855	1.826	1.728	1.606	1.742
8	1.823	1.801	1.559	1.428	1.635
Slope	-0.022	-0.027	-0.055	-0.071	-0.047
Si	0.050	0.061	0.127	0.163	0.107
Fraction retained in the top size at 60% filling of voids with particles					
	-13.2+9.5 mm	-9.5+5.6 mm	-5.6+4 mm	-4+2.8 mm	-2.8+1.18 mm
0	2.000	2.000	2.000	2.000	2.000
0.75	1.989	1.971	1.945	1.909	1.949
2.5	1.964	1.933	1.816	1.725	1.847
5	1.867	1.814	1.632	1.484	1.671
8	1.773	1.768	1.398	1.172	1.384
Slope	-0.029	-0.030	-0.075	-0.102	-0.076
Si	0.067	0.070	0.173	0.236	0.174

7.2. Breakage Function

Table A3 below shows the mass that is broken and remains after breakage at each time intervals and Table A4 shows the data that was used to plot the cumulative breakage parameters for different conditions (Figures 19, 20 and 21 in the main report) which was calculated using the BII method.

Table A3: Size classes for breakage functions estimation

Size classes of products using critical speed at 0.75 min					
Size Class	-13.2+9.5 mm	-9.5+5.6 mm	-5.6+4 mm	-4+2.8 mm	-2.8+1.18 mm
1	4.328	0.000	0.000	0.000	0.000
2	0.371	4.554	0.000	0.000	0.000
3	0.010	0.111	4.323	0.000	0.000
4	0.004	0.026	0.307	3.979	0.000
5	0.006	0.017	0.072	0.674	4.377
6	0.032	0.042	0.048	0.097	0.373
Total	**4.750**	**4.750**	**4.750**	**4.750**	**4.750**
Size classes of products using critical speed at 0.75 min					
Size Class	-13.2+9.5 mm	-9.5+5.6 mm	-5.6+4 mm	-4+2.8 mm	-2.8+1.18 mm
1	4.328	0.000	0.000	0.000	0.000
2	0.371	4.554	0.000	0.000	0.000
3	0.010	0.111	4.323	0.000	0.000
4	0.004	0.026	0.307	3.979	0.000
5	0.006	0.017	0.072	0.674	4.377
6	0.032	0.042	0.048	0.097	0.373
Total	**4.750**	**4.750**	**4.750**	**4.750**	**4.750**
Size classes of products using powder filling at 0.75 min					
Size Class	-13.2+9.5 mm	-9.5+5.6 mm	-5.6+4 mm	-4+2.8 mm	-2.8+1.18 mm
1	3.472	0.000	0.000	0.000	0.000
2	0.049	3.335	0.000	0.000	0.000
3	0.004	0.119	3.138	0.000	0.000
4	0.004	0.037	0.271	2.892	0.000
5	0.006	0.031	0.084	0.516	3.167
6	0.028	0.041	0.070	0.155	0.396
Total	**3.563**	**3.563**	**3.563**	**3.563**	**3.563**

Table A4: Cumulative breakage function for different milling conditions

Cumulative breakage function for reference conditions					
B1,1	1.000	1.000	1.000	1.000	1.000
B2,1	1.000	1.000	1.000	1.000	1.000
B3,1	0.166	1.000	1.000	1.000	1.000
B4,1	0.125	0.443	1.000	1.000	1.000
B5,1	0.105	0.272	0.350	1.000	1.000
B6,1	0.071	0.135	0.155	0.165	1.000
Cumulative breakage function for critical speed					
B1,1	1.000	1.000	1.000	1.000	1.000
B2,1	1.000	1.000	1.000	1.000	1.000
B3,1	0.116	1.000	1.000	1.000	1.000
B4,1	0.094	0.429	1.000	1.000	1.000
B5,1	0.086	0.297	0.272	1.000	1.000
B6,1	0.072	0.208	0.108	0.116	1.000
Cumulative breakage function for powder filling					
B1,1	1.000	1.000	1.000	1.000	1.000
B2,1	1.000	1.000	1.000	1.000	1.000
B3,1	0.459	1.000	1.000	1.000	1.000
B4,1	0.410	0.470	1.000	1.000	1.000
B5,1	0.376	0.309	0.349	1.000	1.000
B6,1	0.308	0.175	0.157	0.213	1.000

7.3. Particle size distribution

Table A5 to A7 shows values that were used to compare product from experiments with estimated product using the population balance equation with estimated selection and breakage functions. This data was used to plot Figures 22, 23 and 24 in the main report.

Table A5: Reference conditions

Reference Conditions			
Feed		Product	
Upper Limit	kg	Experimental	Estimated
13.2	0.79	0.687	0.57
9.5	1.28	1.096	0.92
5.6	1.26	0.533	0.77
4	0.64	0.5	0.52
2.8	0.41	0.728	0.63
1.18	0.24	0.217	0.68
0.85	0.13	0.204	0.27
0.6	0.00	0.785	0.38
Total	**4.75**	**4.75**	**4.75**

Table A6: Change in critical speed conditions

Change in critical Speed			
Feed		Product	
Upper Limit	kg	Experimental	Estimated
13.2	0.68	0.65	0.46
9.5	0.68	0.569	0.49
5.6	0.68	0.259	0.38
4	0.68	0.253	0.39
2.8	0.68	0.414	0.63
1.18	0.68	0.208	1.19
0.85	0.68	0.365	0.84
0.6	0.00	2.032	0.38
Total	**4.75**	**4.75**	**4.75**

Table A7: Change in powder loading conditions

Change in Powder Loading			
Feed		Product	
Upper Limit	kg	Experimental	Estimated
13.2	0.35	0.30	0.25
9.5	0.79	0.64	0.55
5.6	1.75	0.80	0.95
4	0.39	0.60	0.46
2.8	0.26	0.62	0.51
1.18	0.03	0.11	0.38
0.85	0.00	0.08	0.12
0.6	0.00	0.41	0.33
Total	**3.56**	**3.56**	**3.56**

7.4. Model Optimisation

The following Table A8 shows the cumulative percentage passing for the reference conditions as well as the optimal conditions from the ball mill. This data was used to plot Figure 25 in the main report.

A8: Cumulative percentage passing

Cumulative % Passing		
Size class	Reference Conditions	Optimal Conditions
13.2	96%	97%
9.5	89%	93%
5.6	84%	90%
4	80%	88%
2.8	73%	84%
1.18	41%	50%
0.85	26%	31%
0.6	11%	13%
0.15	8%	9%
0.075	0%	0%
0.006	0%	0%

7.5. Spiral Modeling

The following Table A9 shows the calculated densities for each size class for the spiral concentrator modelling. Table A10 shows data that was used to plot Figure 26 in the main report using the single attribute density model while Table A11 shows data that was used to plot Figure 27 in the main report using the Bi-attribute density and size model

A9: Calculated densities for each size class

Upper size limit (mm)	Density (kg/m^3)
13.2	3,589
9.5	3,662
5.6	3,680
4	3,712
2.8	3,732
1.18	3,989
0.85	3,937
0.6	3,807
0.15	3,773
0.075	3,738
0.006	3,722

Table A10: Data used from the single attribute density model

Particle density (kg/m3)	**Partition number (%)**
1000	3%
2000	10%
3000	24%
4000	45%
5000	68%
6000	84%
7000	93%
8000	97%
9000	99%
10000	100%

Table A11: Data used from the Bi-attribute density and size model

	Partition Number (%)				
Particle density (kg/m^3)	**13.2 mm**	**9.5 mm**	**5.6 mm**	**4.0 mm**	**2.8 mm**
750	0%	1%	1%	1%	2%
1500	3%	4%	5%	6%	7%
2250	11%	12%	13%	14%	16%
3000	24%	25%	26%	26%	27%
3750	43%	42%	41%	40%	39%
4500	64%	60%	57%	54%	51%
5250	81%	76%	72%	68%	63%
6000	92%	88%	83%	79%	73%
6750	98%	95%	91%	87%	81%
7500	99%	98%	96%	93%	88%